

# BOUNDED HYPERBOLIC TANGENT: A STABLE AND EFFICIENT ALTERNATIVE TO PRE-LAYER NORMALIZATION IN LARGE LANGUAGE MODELS

Hoyoon Byun<sup>1</sup>, Youngjun Choi<sup>1</sup>, Taero Kim<sup>1</sup>, Sungrae Park<sup>2</sup>, Kyungwoo Song<sup>1\*</sup>

<sup>1</sup>Yonsei University <sup>2</sup>Upstage AI  
 {hoyun.byun, choiyj9803, taero.kim, kyungwoo.song}@yonsei.ac.kr  
 sungrae.park@upstage.ai

## ABSTRACT

Pre-Layer Normalization (Pre-LN) is the de facto choice for large language models (LLMs) and is crucial for stable pretraining and effective transfer learning. However, Pre-LN is inefficient due to repeated statistical calculations and suffers from the curse of depth. As layers grow, the magnitude and variance of the hidden state escalate, destabilizing training. Efficiency-oriented normalization-free methods such as Dynamic Tanh (DyT) improve speed but remain fragile at depth. To jointly address stability and efficiency, we propose Bounded Hyperbolic Tanh (BHyT), a drop-in replacement for Pre-LN. BHyT couples a tanh nonlinearity with explicit, data-driven input bounding to keep activations within a non-saturating range. It prevents depth-wise growth in activation magnitude and variance and comes with a theoretical stability guarantee. For efficiency, BHyT computes exact statistics once per block and replaces a second normalization with a lightweight variance approximation, enhancing efficiency. Empirically, BHyT demonstrates improved stability and efficiency during pretraining, achieving an average of 15.8% faster training and an average of 4.2% higher token generation throughput compared to RMSNorm, while matching or surpassing its inference performance and robustness across language understanding and reasoning benchmarks. Our code is available at: <https://anonymous.4open.science/r/BHyT>

## 1 INTRODUCTION

The remarkable progress of large language models (LLMs) is tightly coupled to the Transformer architecture, where normalization layers play a central role Vaswani et al. (2017). In particular, Pre-Layer Normalization (Pre-LN), which applies normalization before each sublayer, has become the de facto standard Xiong et al. (2020); Radford et al. (2019); Brown et al. (2020); Touvron et al. (2023). This design stabilizes optimization in very deep networks, enabling training at scale and strong transfer performance across diverse tasks. By regulating the scale and distribution of activations, Pre-LN provides a reliable training regime that helps unlock the modern era of large-scale LLMs Ba et al. (2016); Xiong et al. (2020).

As models push to greater depths, however, these foundation models expose a critical weakness. Recent analyses identify a curse of depth, in which the interaction between residual connections and Pre-LN drives rapid, often near-exponential, growth in hidden-state magnitude and variance with layer depth (Sun et al., 2025). This escalation is more important than simple divergence: it drives the block Jacobian toward the identity, so deep layers learn little beyond an expensive identity mapping Sun et al. (2025). The core challenge is thus not merely preventing crashes; it is preserving informative transformations and efficient signal propagation so that every layer contributes meaningfully to learning.

The community has explored remedies along a stability–efficiency axis. On the stability end, stronger normalization seeks to suppress depth-wise drift. For instance, Peri-LN applies normaliza-

---

\*Corresponding author

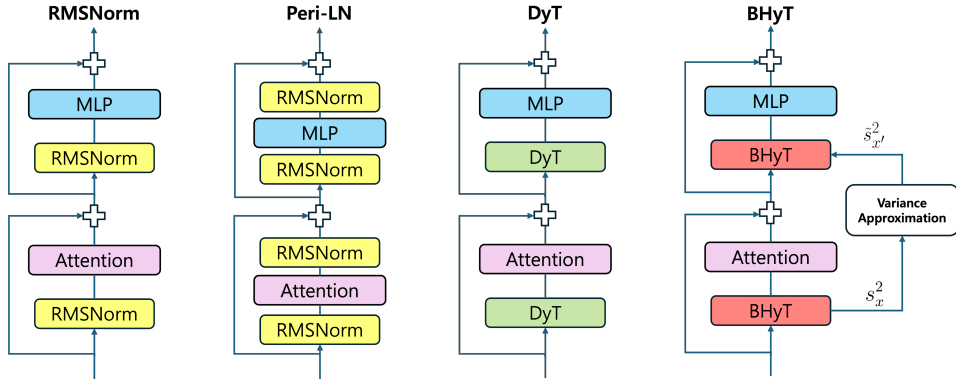


Figure 1: Architectural comparison of normalization strategies in Transformer blocks. **RMSNorm** applies normalization before each sublayer to stabilize activations but suffers from variance growth at scale. **Peri-LN** reinforces stability by normalizing both before and after each sublayer. **DyT** replaces normalization with a lightweight scaled tanh nonlinearity with learnable scalar  $\alpha$ . **BHyT** (ours) combines bounded tanh with data-driven variance control: it computes input variance once per block, approximates subsequent variance for efficiency, and explicitly constrains activations to a non-saturating range, thereby unifying stability and efficiency.

tion both before and after each sublayer, curbing variance growth and maintaining gradient health even at extreme depths Kim et al. (2025). The trade-off is substantial overhead: doubled normalization increases reduction operations and memory traffic, inflating latency. On the efficiency end, RMSNorm removes mean centering to reduce computational costs and has been widely adopted in modern LLMs Zhang & Sennrich (2019). Yet it only partially controls activation statistics and does not fundamentally resolve variance accumulation, leaving depth scaling fragile.

A more radical line of work questions the need for normalization at all. Dynamic Tanh (DyT) replaces normalization with a simple element-wise nonlinearity and a learnable scale Zhu et al. (2025). By eliminating per-token statistics, DyT accelerates both training and inference. However, this efficiency comes with a major risk: activation saturation. When inputs grow large, precisely the hazard under depth, the nonlinearity saturates, gradients vanish, and optimization becomes brittle. Relying on a learned global scale to self-regulate these dynamics is often insufficient in the face of strong depth-induced amplification.

This landscape reveals a clear gap: methods that guarantee stability typically sacrifice efficiency, while efficient methods fail to robustly address the curse of depth (Sun et al., 2025). What is needed is a mechanism that retains the simplicity and throughput of normalization-free designs while providing principled control over depth-wise growth.

We introduce Bounded Hyperbolic Tanh (BHyT) to close this gap. As shown in Figure 1, BHyT is a drop-in replacement for Pre-LN that couples a tanh nonlinearity with explicit, data-driven input bounding. By keeping activations within a non-saturating regime with high probability, BHyT prevents depth-wise growth in activation magnitude and variance, preserving informative transformations as depth increases. Beyond this forward-path protection, BHyT provides a theoretical stability guarantee regarding variance propagation. Specifically, for a network of depth  $L$ , the output variance of BHyT is provably smaller than that of LayerNorm Scaling (LNS) (Sun et al., 2025) under specific hyperparameter conditions. This ensures that BHyT more effectively suppresses depth-wise variance growth compared to existing stable normalization methods, thereby mitigating the curse of depth (Sun et al., 2025) even in very deep architectures. To minimize overhead, BHyT computes exact statistics once per block and replaces a second normalization with a lightweight variance approximation that tracks attention-induced variation, reducing reductions and memory movement. The result is a practical module that maintains stability without reintroducing the throughput penalties of heavy normalization.

Empirically, BHyT stabilizes pretraining for deeper LLMs, improves training and inference throughput, and yields stronger transfer performance, indicating that curbing depth-wise variance growth translates into better generalization.

Our contributions are summarized as follows.

- We propose BHyT, a principled, plug-and-play alternative to Pre-LN that unifies stability with efficiency by bounding activations to a non-saturating range.
- We develop an efficient approximation that computes statistics once per block and uses a lightweight variance approximation to avoid additional reductions, thereby improving throughput.
- We present comprehensive experiments demonstrating stable depth scaling, faster training and inference, and improved downstream task performance.

## 2 RELATED WORKS

### 2.1 LIMITATIONS OF PRE-LAYER NORMALIZATION

Layer normalization has been a key component in Transformer architectures (Ba et al., 2016), and its Pre-LN variant has become the default in most LLMs (Xiong et al., 2020). The Pre-LN design, which normalizes hidden states before attention and feed-forward layers, improves stability when training begins. Still, this design is not without drawbacks. From a stability perspective, recent studies have shown that Pre-LN suffers from massive activations as depth increases (Sun et al., 2025; Kim et al., 2025). In this regime, the mean and variance of hidden states grow rapidly across layers, destabilizing optimization. From an efficiency perspective, normalization requires computing statistics such as the mean and variance of activations. These reductions introduce latency and memory overhead, which accumulate as depth increases. As a result, Pre-LN can both destabilize very deep models and become a bottleneck for training throughput and scalability.

### 2.2 NORMALIZATION-BASED ENHANCEMENTS

The main bottleneck of normalization-based designs lies in the repeated computation of statistics at every block. A first attempt to reduce this cost was RMSNorm, which discards the mean and normalizes only by the root mean square of activations (Zhang & Sennrich, 2019). This removes part of the overhead while keeping activations within a reasonable range. However, variance computation is still required for every layer, and the instability of Pre-LN remains unresolved.

To address this instability, LayerNorm Scaling (LNS) (Sun et al., 2025) introduces a layer-index scaling that constrains variance growth across depth. By rescaling activations according to layer-index, it alleviates the massive activation problem and stabilizes optimization in very deep networks. Although LNS improves stability, its reliance on per-block statistics keeps the cost high in large-scale training. Peri-LN reinforces stability further by applying normalization both before and after each sublayer (Kim et al., 2025). This suppresses variance spikes and improves convergence and downstream accuracy; however, doubling normalization operations adds substantial overhead, making it less suitable for large-scale pretraining.

### 2.3 NORMALIZATION-FREE ALTERNATIVES

To avoid the overhead of statistical computations altogether, recent work has explored removing normalization. DyT follows this direction by replacing RMSNorm with a bounded activation function,  $\tanh(\alpha_{\text{DyT}}x)$ , where  $\alpha_{\text{DyT}}$  is a learnable scalar (Zhu et al., 2025). This eliminates the need for mean or variance estimation, improving both training and inference speeds. The  $\tanh$  function ensures that activations remain bounded, and the learnable scalar  $\alpha_{\text{DyT}}$  rescales inputs so that the effective range of  $\tanh$  is better utilized.

Although DyT improves efficiency, it does not control how the output mean and variance grow with depth. Moreover, its learnable scalar parameter  $\alpha_{\text{DyT}}$  is not explicitly designed for stability. It only rescales the inputs indirectly, without actively suppressing variance escalation in deep networks. As a result, its training stability at scale is not explicitly guaranteed and may be more susceptible to saturation-induced gradient vanishing and related instabilities than normalization-based methods.

In contrast to DyT, BHyT explicitly guarantees stability by constraining variance growth. To address the computational bottleneck of the required statistical calculations, we introduce a variance approximation mechanism. This design effectively harmonizes robust training stability with the high efficiency of normalization-free architectures.

### 3 METHODOLOGY

An ideal normalization scheme should allow for controlled, sub-exponential or linear growth of variance (Sun et al., 2025; Kim et al., 2025), sufficient to preserve signal propagation without leading to explosive instability. To this end, we introduce BHyT, a novel normalization layer designed to achieve both stability and speed. BHyT builds upon the efficiency of methods like DyT, which use S-shaped functions (e.g.,  $\tanh$ ) to bypass explicit statistical computation. However, DyT’s reliance on a single learnable scalar to control the input to  $\tanh$  offers no explicit guarantee against saturation, which can lead to vanishing gradients in very deep models. BHyT addresses this limitation by explicitly bounding the input to the nonlinear function, ensuring both numerical stability and a well-behaved gradient flow.

#### 3.1 ENSURING STABILITY VIA INPUT BOUNDING

To prevent the saturation of the  $\tanh$  function and ensure stable gradient flow, BHyT explicitly constrains its input to lie within a predefined range  $(-\lambda, \lambda)$  with high probability. Rather than enforcing this constraint deterministically, we adopt a probabilistic perspective that leverages the first- and second-order statistics of the input distribution.

Specifically, we utilize Chebyshev’s inequality, which guarantees that for any random variable  $X$  with a finite mean  $\mu$  and variance  $s^2$ , the probability of deviating from the mean by less than  $\kappa$  standard deviations is at least  $1 - 1/\kappa^2$  (i.e.,  $P(|X - \mu| \leq \kappa s) \geq 1 - \kappa^{-2}$ ).

Motivated by this distribution-agnostic bound, we define a formulation BHyT\* that explicitly incorporates these statistics. Given an input  $x \in \mathbb{R}^d$  with a mean  $\mu_x$  and a standard deviation  $s_x$ , BHyT\* rescales  $x$  such that the argument of  $\tanh(\cdot)$  falls within  $(-\lambda, \lambda)$  with probability at least  $1 - \kappa^{-2}$ :

$$\text{BHyT}^*(x) = \gamma \odot \tanh\left(\frac{\lambda}{\kappa s_x + |\mu_x|} x\right). \quad (1)$$

Where  $\gamma \in \mathbb{R}^d$  is a learnable scale parameter,  $\odot$  denotes the element-wise product,  $\lambda > 0$  is a hyperparameter defining the range of the bound, and  $\kappa = (1 - p)^{-1/2}$  is derived from a target probability  $p \in (0, 1)$  as shown in Proposition 3.1, whose proof is detailed in Appendix B.1.

**Proposition 3.1** (Input scaling bound at the level  $p$ ). *Let  $x \in \mathbb{R}$  with  $\mathbb{E}[x] = \mu_x$  and  $\text{Var}(x) = s_x^2$ . Given a predefined bound  $\lambda > 0$  and target probability  $p \in (0, 1)$ , if  $\alpha = \frac{\lambda}{\kappa s_x + |\mu_x|}$ , then  $P(|\alpha x| \leq \lambda) \geq p$  for any distribution with finite variance, where  $\kappa := (1 - p)^{-1/2}$ .*

**Remark 3.2.** For  $p = 0.99$ ,  $\kappa = 10$  and  $\alpha = \lambda/(|\mu_x| + 10s_x)$ .

#### 3.2 ACCELERATING BHyT WITH VARIANCE APPROXIMATION

A key strategy for accelerating Transformer models is to replace standard LN (e.g., RMSNorm) with a  $\tanh$  function. This approach can significantly improve computational speed by eliminating the need for explicit statistical calculations inherent in layers like RMSNorm. However, BHyT\*, which requires the per-instance calculation of mean and variance, would lose this speed advantage. Motivated by this, we introduce BHyT, an approximate variant of BHyT\*. Although closely related to BHyT\*, BHyT employs variance approximation, thereby enhancing both stability and efficiency.

Our solution, BHyT, successfully navigates this trade-off by approximating the variance instead of computing it directly. To illustrate its efficiency, while a standard Transformer block computes statistics twice (e.g., via RMSNorm), BHyT requires only a single direct variance calculation at the entrance of the block. All subsequent variances for intermediate states are approximated. This drastic reduction in statistical overhead leads to substantial speed improvements. As with RMSNorm, BHyT assumes a zero-mean input, which eliminates the need for explicit mean computation.

##### 3.2.1 BHyT BEFORE THE ATTENTION LAYER

For the first normalization within a block, BHyT directly computes the variance of the input tensor  $x$  across the feature dimension. The BHyT is then applied as follows:

**Algorithm 1** Transformer Decoder Block with BHyT

---

```

1: Input: Token embedding  $x \in \mathbb{R}^d$ 
2: Hyperparameters:  $\lambda_{\text{Attn}}, \lambda_{\text{MLP}}, \kappa > 0$ , Sequence length  $T$ 
3: Learnable Parameters: Scale parameter  $\gamma_{\text{Attn}}, \gamma_{\text{MLP}} \in \mathbb{R}^d$ 
4: Weights:  $W_V \in \mathbb{R}^{d \times d_V}$ ,  $W_O \in \mathbb{R}^{d_V \times d}$ ,  $W_1 \in \mathbb{R}^{d \times d_m}$ ,  $W_2 \in \mathbb{R}^{d_m \times d}$ 
5: Output:  $x_{\text{out}} \in \mathbb{R}^d$ 
6:  $s_x^2 \leftarrow \frac{1}{d} \sum_{j=1}^d x_j^2$  ▷ Input variance
7: parallel do
  (A) Variance-approximation
   $\tilde{s}_{x'}^2 \leftarrow s_x^2 + \frac{1}{Td} \|W_V W_O\|_F^2 \left(\frac{\lambda_{\text{Attn}}}{\kappa}\right)^2$ 

  (B) Attention path
  # BHyT before attention
   $s_x \leftarrow \sqrt{\tilde{s}_x^2}$ 
   $\alpha_{\text{Attn}} \leftarrow \frac{\lambda_{\text{Attn}}}{\kappa \cdot s_x}$ 
   $z_{\text{Attn}} \leftarrow \gamma_{\text{Attn}} \odot \tanh(\alpha_{\text{Attn}} \cdot x)$  ▷ BHyTAttn
   $h_{\text{Attn}} \leftarrow \mathcal{A}(z_{\text{Attn}}; W_V, W_O)$  ▷ Attention sublayer
8: end parallel

9:  $x' \leftarrow x + h_{\text{Attn}}$  ▷ Residual connection
  # BHyT before MLP
10:  $\tilde{s}_{x'}^2 \leftarrow \sqrt{\tilde{s}_{x'}^2}$ 
11:  $\alpha_{\text{MLP}} \leftarrow \frac{\lambda_{\text{MLP}}}{\kappa \cdot \tilde{s}_{x'}}$ 
12:  $z_{\text{MLP}} \leftarrow \gamma_{\text{MLP}} \odot \tanh(\alpha_{\text{MLP}} \cdot x')$  ▷ BHyTMLP
13:  $h_{\text{MLP}} \leftarrow \text{MLP}(z_{\text{MLP}}; W_1, W_2)$  ▷ MLP sublayer
14:  $x_{\text{out}} \leftarrow x' + h_{\text{MLP}}$ 
15: return  $x_{\text{out}}$  ▷ Residual connection

```

---

$$z_{\text{Attn}} = \text{BHyT}_{\text{Attn}}(x) = \gamma_{\text{Attn}} \odot \tanh\left(\frac{\lambda_{\text{Attn}}}{\kappa s_x} x\right) \quad (2)$$

where  $s_x^2$  denotes the per-instance variance calculation and  $\lambda_{\text{Attn}}$  denotes the predefined range for  $\text{BHyT}_{\text{Attn}}$ . The output  $z_{\text{Attn}}$  is then passed to the self-attention layer,  $\mathcal{A}(\cdot)$ , which produces the attention output  $h_{\text{Attn}} = \mathcal{A}(z_{\text{Attn}})$ .

### 3.2.2 BHyT BEFORE THE MLP LAYER

Let  $x' = x + h_{\text{Attn}}$  be the output of the first residual connection and the input to the second BHyT (i.e.,  $\text{BHyT}_{\text{MLP}}$ ). Instead of re-computing the variance of  $x'$ , which is computationally expensive, we approximate it as

$$\tilde{s}_{x'}^2 = s_x^2 + \tilde{s}_{h_{\text{Attn}}}^2. \quad (3)$$

As shown in Equation 3, our approximation for the intermediate variance,  $\tilde{s}_{x'}^2$ , is the sum of two components. The first term,  $s_x^2$ , is the variance of the Transformer block's input, reused directly from the preceding  $\text{BHyT}_{\text{Attn}}$  computation. The second term,  $\tilde{s}_{h_{\text{Attn}}}^2$ , is our efficient approximation of the variance contributed by the attention layer's output. Similarly to Equation 2,  $\text{BHyT}_{\text{MLP}}$  then utilizes this approximated variance.

It allows BHyT to maintain normalization stability while minimizing the overhead from repeated statistical calculations within a single Transformer block.

**Assumption 3.3.** Let the sequence length  $T$  be sufficiently large so that the attention weights can be treated as approximately uniform (Ledoux, 2001). Let the token-level activation  $x \in \mathbb{R}^d$  and the projection matrices  $W_V$  and  $W_O$  follow independent zero-mean normal distributions. By these

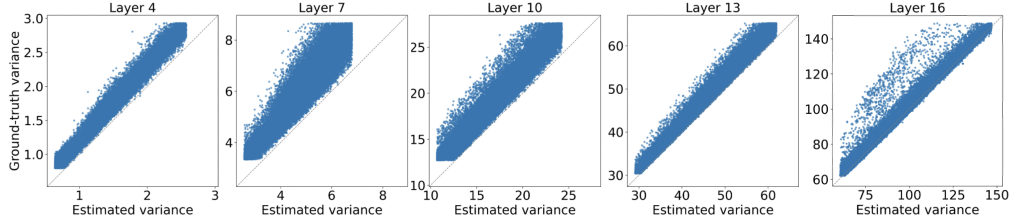


Figure 2: Approximated and ground-truth activation variances for the second  $\text{BHyT}_{\text{MLP}}$  layer across different Transformer blocks in Llama-1B. The variance estimates are evaluated using 100 randomly sampled inputs from the C4 training corpus. The diagonal line represents the ideal  $y = x$  reference. Deeper layers exhibit closer alignment with this reference, indicating improved approximation accuracy. Complete results for all 16 layers are reported in the Appendix D.3.

assumptions,  $\text{BHyT}$  keeps the argument of the  $\tanh(\cdot)$  function in its near-linear regime, such that scaling by  $\lambda/\kappa s_x$  directly yields a variance of approximately  $\lambda^2/\kappa^2$ .

**Theorem 3.4** (Variance approximation of attention output). *Under Assumption 3.3, let  $h_{\text{Attn}} \in \mathbb{R}^d$  denote the output vector of the attention layer. The average coordinate-wise variance of the output, denoted by  $\tilde{s}_{h_{\text{Attn}}}^2 := \frac{1}{d} \sum_{k=1}^d \text{Var}((h_{\text{Attn}})_k)$ , is approximated as:*

$$\tilde{s}_{h_{\text{Attn}}}^2 \approx \frac{1}{Td} \|W_V W_O\|_F^2 \cdot \frac{\lambda_{\text{Attn}}^2}{\kappa^2}. \quad (4)$$

Note that  $\tilde{s}_{h_{\text{Attn}}}^2$  represents the expected variance derived from the model parameters. Crucially, in high-dimensional spaces (large  $d$ ), the concentration of measure phenomenon ensures that the actual sample variance of an individual activation vector converges to this expected value. This justifies using the theoretical expectation as a reliable and efficient proxy for the instance-wise variance.

Theorem 3.4 demonstrates that the variance induced by the attention module can be approximated solely using model characteristics—such as the attention layer weights, sequence length, and  $\text{BHyT}$  parameters— independent of input values. The detailed proof is provided in Appendix B.2. This independence allows the variance approximation to be computed in parallel with the forward path, effectively reducing the latency overhead associated with statistical calculations. As shown in Figure 2, our approximated variance aligns closely with the actual variance of intermediate hidden states. Algorithm 1 details this parallelized process within the Transformer block.

In particular, during inference,  $W_V$  and  $W_O$  are fixed after training and can be loaded once with the model, so the proposed variance approximation introduces no additional bottleneck in the inference path. During training, we further minimize overhead by updating  $W_V$  and  $W_O$  only at a fixed interval (i.e., periodically rather than at every step), which reduces the frequency of recomputation and keeps the training-speed bottleneck negligible.

### 3.3 DEPTH-WISE VARIANCE PROPAGATION AND STABILITY OF $\text{BHyT}$

**Theorem 3.5** (Finite-depth variance bound of  $\text{BHyT}$ ). *For a network of depth  $L$ , if the  $\text{BHyT}$  hyperparameters satisfy  $\frac{\lambda}{\kappa} < \frac{1}{\sqrt{L}}$ , then the output variance of  $\text{BHyT}$  is strictly smaller than that of LNS (Sun et al., 2025) for every layer  $\ell$  up to depth  $L$  (i.e., for all  $1 \leq \ell \leq L$ ):*

$$\tilde{s}_{x_\ell}^{\text{BHyT}} < \tilde{s}_{x_\ell}^{\text{LNS}}, \quad \forall \ell \in \{1, \dots, L\}. \quad (5)$$

Theorem 3.5 gives a finite-depth variance bound for  $\text{BHyT}$ : if  $\lambda/\kappa < 1/(\sqrt{L})$ , then for every layer  $\ell < L$ , the variance multiplier of  $\text{BHyT}$  is no larger than that of LNS, so the output variance at depth  $L$  is smaller. For example, choosing  $\lambda = 1$  and  $\kappa = 10$  yields  $L \approx 100$ , up to which  $\text{BHyT}$  has a smaller output variance than LNS. This suggests that, for typical model depths,  $\text{BHyT}$  can be more stable than LNS in terms of variance growth. The detailed proof is provided in Appendix B.4.5

## 4 EXPERIMENTS & RESULTS

In this section, we present a comprehensive set of experiments designed to evaluate the effectiveness of our proposed method, BHyT. Our evaluation is structured around three primary objectives: 1) **Stability**, assessing BHyT’s ability to mitigate the “curse of depth” (Sun et al., 2025) by analyzing activation growth across layers; 2) **Efficiency**, comparing its computational throughput against existing normalization methods; and 3) **Performance**, measuring its effectiveness in both pretraining and supervised fine-tuning (SFT) contexts to ensure it achieves competitive results.

### 4.1 EXPERIMENTAL SETUP

**Models.** We conduct experiments with two model scales from the Llama-3.2 family: a 1B-parameter model with 16 layers and a 3B-parameter model with 28 layers. We instantiate only the architectures and train all models from scratch. This setup allows us to explicitly examine the effect of increasing model depth on stability and efficiency and to highlight the scalability benefits of our proposed BHyT method.

**Training data and protocols.** Pretraining is performed on the C4 corpus, a large-scale English text dataset widely used in language model pretraining (Raffel et al., 2020). For supervised fine-tuning (SFT), we employ an instruction-tuning dataset: Lima1k (Zhou et al., 2023), which contains carefully curated, high-quality instructions that provide broader coverage with a larger number of instruction–response pairs. This combination enables us to evaluate both high-quality, low-resource, and large-scale instruction-tuning scenarios.

Following pretraining and SFT, we assess model performance on a diverse suite of seven language understanding and reasoning benchmarks: ARC-e (Clark et al., 2018), PIQA (Bisk et al., 2020), HellaSwag (Zellers et al., 2019), OpenBookQA (Mihaylov et al., 2018), Winogrande (Sakaguchi et al., 2021), MMLU (Hendrycks et al., 2020), and BoolQ (Clark et al., 2019). These benchmarks collectively evaluate both factual knowledge and reasoning abilities. We report task-specific accuracy and macro-average accuracy across tasks as the primary evaluation metric.

**Frameworks and tooling.** All pretraining and SFT experiments are implemented using the Llama Factory framework (Zheng et al., 2024), which provides efficient fine-tuning utilities and ensures consistent implementation across methods. For downstream evaluation, we use the lm-evaluation-harness toolkit (Gao et al., 2024), adopting its standardized task configurations to ensure comparability with prior work. Accuracy scores are computed directly by the harness without modification, ensuring the reproducibility of reported results.

**Hyperparameter setup.** We select hyperparameters from a shared sweep range to ensure a fair comparison across all methods. Each method identifies its optimal configuration by choosing the hyperparameters that yield the lowest evaluation loss after the pretrained C4 datasets reach 20K steps, and we use this configuration for the full training. The detailed hyperparameter search ranges, the final selected configuration for each method, and the full experimental setup—including hardware and parallelism strategy—are provided in the Appendix C.

### 4.2 PRETRAINING LLMs

We compare BHyT against several baselines: RMSNorm (Zhang & Sennrich, 2019), the default normalization used in the Llama family; LNS (Sun et al., 2025) and Peri-LN (Kim et al., 2025), both designed to enhance training stability; and DyT (Zhu et al., 2025), which replaces the conventional Pre-LN with a  $\tanh(\cdot)$ -based function having learnable scalar parameter  $\alpha_{\text{DyT}}$ . We conducted pretraining on the C4 dataset. The 1B model was optimized with a sequence length of 1024, a batch size of 32, and for 50,000 steps, amounting to  $\sim 1.64\text{B}$  tokens. The 3B model used the same configuration but was trained for 60,000 steps, resulting in  $\sim 1.97\text{B}$  tokens. To further evaluate each method under a more realistic large-scale setting, we additionally extend the pretraining budget to 20B tokens and conduct experiments on both the 1B and 3B models.

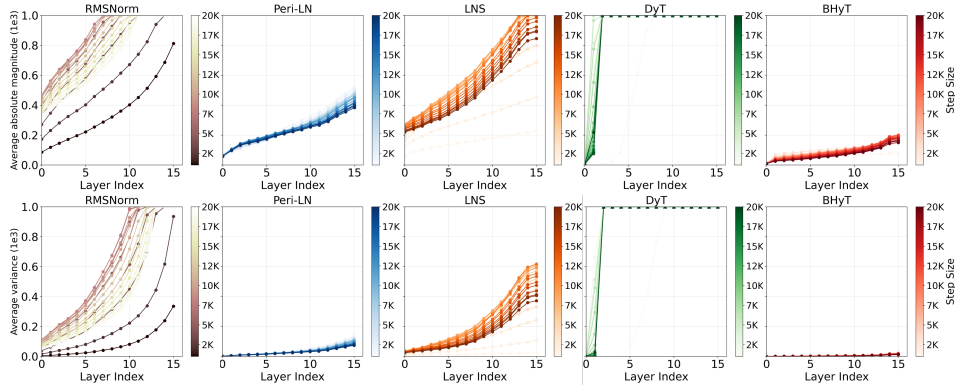


Figure 3: Layer-wise analysis of output statistics on the Llama-1B model. The top row shows the average absolute magnitude of activations, and the bottom row shows the average layer-wise variance. RMSNorm and DyT exhibit rapid growth with depth, reflecting the curse of depth and instability in deeper networks. LNS and Peri-LN suppress this escalation, and BHyT further stabilizes activation variability, yielding lower magnitude and variance than LNS.

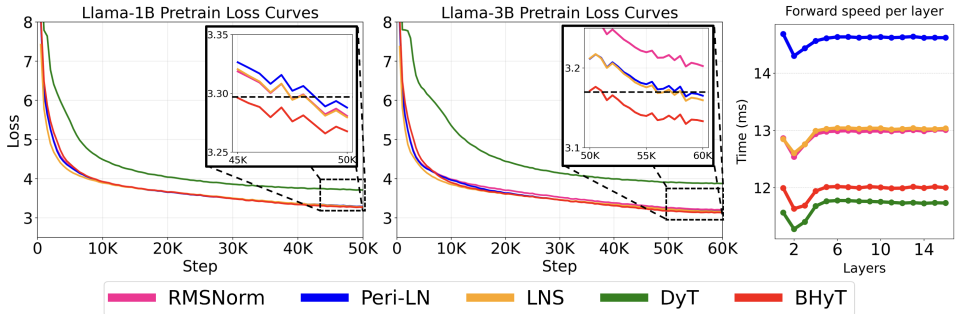


Figure 4: Pretraining performance and forward speed comparison. The first two figures denote loss curves for Llama-1B and Llama-3B, respectively. These show that BHyT achieves stable and competitive convergence, surpassing normalization-based baselines. Notably, compared to normalization-based baselines, BHyT reaches the same loss level fastest towards the end of training. The rightmost figure denotes the Llama-1B forward path speed comparison, highlighting that DyT is the fastest, whereas Peri-LN is the slowest. Overall, BHyT provides the best trade-off, combining reliable convergence with high training efficiency.

Figure 3 presents the layer-wise evolution of activation magnitude and variance for the Llama-1B model<sup>1</sup>. RMSNorm shows clear instability, with both quantities increasing rapidly with depth. DyT shows a similar trend, suffering from explosive growth in deeper layers; notably, we observed that DyT’s training stability is highly sensitive to the learning rate (see Appendix D.2). In contrast, similar to Peri-LN and LNS, BHyT demonstrates a controlled, linear increase in statistics across layers. However, BHyT is distinguished by a noticeably gentler slope compared to these baselines, effectively suppressing depth-wise drift. This behavior leads to more stable optimization while retaining efficiency.

Figure 4 shows the pretraining loss curves for Llama-1B and Llama-3B, alongside the forward pass speed per layer. The results demonstrate that BHyT achieves stable and competitive convergence, notably reaching the target loss level faster than normalization-based baselines towards the end of training. Besides, BHyT significantly outperforms the slower Peri-LN by approximately 17.7% and demonstrates 7.7% faster forward computation than RMSNorm. Consequently, BHyT provides the best trade-off, combining reliable convergence with high training efficiency.

<sup>1</sup>To ensure a fair comparison, we evaluate all methods under a fixed hyperparameter setting (Learning rate:  $3e-4$ , Warm-up ratio:  $1e-1$ ) at 20K training steps.

Table 1: Pretraining (PT)-only evaluation for Llama-3B; downstream benchmarks in a 5-shot setting, averaged over five training seeds. The results demonstrate that BHyT achieves performance comparable to or superior to strong baselines while maintaining high computational speed. PPL denotes the perplexity score.

Llama-3B											
Method	PT Train Loss	PT Eval Loss	PT Eval PPL	Arc-e	PIQA	Hellaswag	OpenBookQA	Winogrande	MMLU	BoolQ	Avg.
RMSNorm	3.203	3.180	24.040	31.01 $\pm$ 0.21	<b>66.57</b> $\pm$ 0.41	<b>41.52</b> $\pm$ 0.25	<b>33.92</b> $\pm$ 0.33	50.50 $\pm$ 0.78	25.67 $\pm$ 0.02	37.94 $\pm$ 0.12	40.89 $\pm$ 0.18
Peri-LN	3.165	3.142	23.156	31.82 $\pm$ 0.38	64.52 $\pm$ 0.24	36.05 $\pm$ 0.11	32.28 $\pm$ 0.59	49.30 $\pm$ 0.52	25.99 $\pm$ 0.00	57.46 $\pm$ 0.31	42.49 $\pm$ 0.25
LNS	3.160	3.139	23.091	<b>31.88</b> $\pm$ 0.42	64.68 $\pm$ 0.46	36.25 $\pm$ 0.10	32.45 $\pm$ 0.53	51.18 $\pm$ 0.75	<b>26.87</b> $\pm$ 0.01	37.83 $\pm$ 0.08	41.16 $\pm$ 0.11
DyT	3.877	3.855	47.244	27.69 $\pm$ 0.27	59.20 $\pm$ 0.15	25.96 $\pm$ 0.17	31.85 $\pm$ 0.38	49.17 $\pm$ 1.28	25.87 $\pm$ 0.02	48.05 $\pm$ 0.56	38.26 $\pm$ 0.12
BHyT	<b>3.133</b>	<b>3.107</b>	<b>22.346</b>	31.84 $\pm$ 0.15	65.08 $\pm$ 0.39	36.48 $\pm$ 0.04	31.76 $\pm$ 0.33	<b>51.62</b> $\pm$ 0.66	25.70 $\pm$ 0.01	<b>60.84</b> $\pm$ 0.29	<b>43.33</b> $\pm$ 0.16

Table 1 shows the pretraining evaluation results, including training loss. The results confirm that BHyT consistently achieves the lowest pretraining loss and superior average accuracy, validating its robust scalability and performance advantage.

Table 2: Supervised fine-tuning (SFT) results across five training seeds for Llama-3B. Reported values include SFT losses and 5-shot downstream benchmark accuracies; BHyT attains lower SFT loss and competitive performance, indicating effective transfer of its pretraining stability to instruction-tuned settings.

Llama-3B											
Method	PT Eval Loss	SFT Train Loss	SFT Eval Loss	Arc-e	PIQA	Hellaswag	OpenBookQA	Winogrande	MMLU	BoolQ	Avg.
RMSNorm	3.272	2.646 $\pm$ 0.011	3.217 $\pm$ 0.130	<b>37.67</b> $\pm$ 0.23	66.96 $\pm$ 0.29	31.70 $\pm$ 0.12	31.12 $\pm$ 0.18	<b>51.22</b> $\pm$ 1.60	22.95 $\pm$ 0.04	53.31 $\pm$ 2.02	39.83 $\pm$ 0.21
Peri-LN	3.279	<b>2.614</b> $\pm$ 0.011	3.178 $\pm$ 0.132	36.80 $\pm$ 0.27	<b>67.05</b> $\pm$ 0.12	<b>37.13</b> $\pm$ 0.09	<b>31.44</b> $\pm$ 0.61	49.06 $\pm$ 0.40	22.94 $\pm$ 0.02	52.75 $\pm$ 1.54	42.45 $\pm$ 0.28
LNS	3.271	2.652 $\pm$ 0.011	3.157 $\pm$ 0.132	34.49 $\pm$ 0.17	65.59 $\pm$ 0.16	37.12 $\pm$ 0.09	28.96 $\pm$ 0.54	50.61 $\pm$ 0.55	22.99 $\pm$ 0.02	52.69 $\pm$ 0.66	41.78 $\pm$ 0.20
DyT	3.855	3.361 $\pm$ 0.010	3.971 $\pm$ 0.132	29.78 $\pm$ 0.40	58.42 $\pm$ 0.53	25.95 $\pm$ 0.17	28.28 $\pm$ 0.90	49.53 $\pm$ 0.79	<b>23.46</b> $\pm$ 0.13	56.64 $\pm$ 1.02	38.87 $\pm$ 0.17
BHyT	<b>3.254</b>	2.693 $\pm$ 0.012	<b>3.130</b> $\pm$ 0.133	34.61 $\pm$ 0.20	66.47 $\pm$ 0.27	36.95 $\pm$ 0.12	29.68 $\pm$ 0.46	51.14 $\pm$ 1.02	23.07 $\pm$ 0.05	<b>58.21</b> $\pm$ 0.81	<b>42.88</b> $\pm$ 0.19

### 4.3 INSTRUCTION FINE-TUNING AND BENCHMARK EVALUATION

We apply LoRA-based supervised fine-tuning to assess whether the stability achieved during pretraining carries over to instruction-tuned performance. Table 2 summarizes the SFT losses and downstream benchmark accuracies for the Llama-3B. Across both scales, BHyT maintains the stable optimization observed during pretraining and transfers this advantage effectively to the SFT stage. Notably, BHyT attains lower SFT loss and competitive accuracy on a broad set of benchmarks, demonstrating that its depth-wise stability and controlled activation dynamics continue to support reliable adaptation beyond pretraining. We present the pretraining and SFT results for the 1B model in Appendix E.

### 4.4 INFERENCE SPEED AND THROUGHPUT ANALYSIS

To evaluate practical deployment efficiency, we benchmark generation throughput using a Hugging Face-based serving framework. We fixed the input length at 512 tokens and measured generation speeds across varying max new token lengths (128, 512, and 1024) with a maximum sequence length of 4096 for Llama-1B.

Table 3 presents the results, where values represent the mean  $\pm$  standard deviation across five trials, and percentages in parentheses denote the relative speed difference compared to BHyT.

BHyT demonstrates superior efficiency compared to standard normalization layers. At 128 output tokens, BHyT (53.5 tokens/s) is approximately 5.6% faster than RMSNorm and 12.9% faster than Peri-LN, effectively mitigating the overhead often associated with advanced normalization techniques. Complete results are provided in Appendix D.4

Table 3: Comparison of generation throughput (tokens/s)

Tokens per second		
RMSNorm	50.5 $\pm$ 1.1	(-5.6%)
Peri-LN	46.6 $\pm$ 0.7	(-12.9%)
LNS	50.6 $\pm$ 0.5	(-5.4%)
DyT	55.6 $\pm$ 0.2	(+3.9%)
BHyT	53.5 $\pm$ 0.4	

Table 4: Performance of Llama-3B pretrained on 20B tokens, evaluated before and after supervised fine-tuning (SFT). BHyT consistently outperforms the stability-oriented baseline, Peri-LN, achieving lower losses and higher downstream accuracy.

Llama-3B (Pretrained on 20B tokens only)													
Method	PT Train Loss	PT Eval Loss	PT Wall time	SFT Tr Loss	SFT Eval Loss	Arc-e	PIQA	Hellaswag	OpenBookQA	Winogrande	MMLU	BoolQ	Avg.
Peri-LN	2.811	2.812	238h	-	-	41.03 $\pm$ 0.56	68.93 $\pm$ 0.67	47.47 $\pm$ 0.21	30.64 $\pm$ 0.99	51.70 $\pm$ 0.26	27.02 $\pm$ 0.00	47.19 $\pm$ 0.74	44.85 $\pm$ 0.27
BHyT	<b>2.756</b>	<b>2.760</b>	<b>171.4h</b>	-	-	<b>45.93</b> $\pm$ 0.46	<b>70.09</b> $\pm$ 0.14	<b>50.97</b> $\pm$ 0.14	<b>31.32</b> $\pm$ 1.00	<b>52.12</b> $\pm$ 0.72	<b>27.62</b> $\pm$ 0.00	<b>55.69</b> $\pm$ 0.86	<b>47.68</b> $\pm$ 0.50
Llama-3B (Pretrained on 20B tokens & SFT)													
Peri-LN	2.811	2.812	238h	2.477 $\pm$ 0.011	2.830 $\pm$ 0.10	50.19 $\pm$ 0.34	70.93 $\pm$ 0.36	48.39 $\pm$ 0.15	<b>31.00</b> $\pm$ 0.58	51.98 $\pm$ 0.64	26.36 $\pm$ 0.11	42.43 $\pm$ 0.99	45.90 $\pm$ 0.21
BHyT	<b>2.756</b>	<b>2.760</b>	<b>171.4h</b>	<b>2.468</b> $\pm$ 0.011	<b>2.764</b> $\pm$ 0.10	<b>53.83</b> $\pm$ 0.38	<b>72.36</b> $\pm$ 0.43	<b>51.62</b> $\pm$ 0.15	30.60 $\pm$ 0.57	<b>53.07</b> $\pm$ 0.47	<b>26.82</b> $\pm$ 0.10	<b>49.89</b> $\pm$ 1.51	<b>48.31</b> $\pm$ 0.27

#### 4.5 ANALYSIS ON SCALABILITY AND GENERALIZATION

To validate BHyT in a more realistic pretraining setting, we extended training to 20B tokens and compared BHyT against Peri-LN. Table 4 reports results for both pretraining-only and post-SFT stages. BHyT achieves lower pretraining loss and perplexity, indicating that our method effectively suppresses depth-wise drift even with larger budgets. Additional results for the 1B model trained on 20B tokens can be found in Appendix E.1.

#### 4.6 ABLATION ON VARIANCE APPROXIMATION

Table 5: Impact of variance approximation on training efficiency and performance. We compare the exact variance calculation baselines (RMSNorm, BHyT\*) against their approximation counterparts (RMSNorm-Approx, BHyT). The results indicate that the approximation mechanism consistently boosts training speed (step/s) across architectures with negligible degradation in convergence and downstream accuracy.

Llama-1B	Variance Approx.	PT Train Loss	PT Eval Loss	PT Eval PPL	Train steps per sec.	Arc-e	PIQA	Hellaswag	OpenBookQA	Winogrande	MMLU	BoolQ	Avg.
RMSNorm	X	3.281	3.272	26.353	0.346	30.97 $\pm$ 0.20	62.89 $\pm$ 0.74	32.77 $\pm$ 0.09	32.32 $\pm$ 0.94	50.54 $\pm$ 0.48	25.70 $\pm$ 0.01	56.26 $\pm$ 0.44	41.64 $\pm$ 0.10
BHyT*	X	<b>3.266</b>	<b>3.254</b>	<b>25.885</b>	0.335	<b>39.82</b> $\pm$ 0.52	<b>64.86</b> $\pm$ 0.50	<b>35.67</b> $\pm$ 0.15	27.68 $\pm$ 0.93	50.40 $\pm$ 0.80	25.19 $\pm$ 0.00	55.34 $\pm$ 0.67	<b>42.71</b> $\pm$ 0.15
RMSNorm-Approx	O	3.293	3.284	26.672	0.381	31.15 $\pm$ 0.44	61.98 $\pm$ 0.57	31.93 $\pm$ 0.04	33.08 $\pm$ 0.04	<b>50.67</b> $\pm$ 0.94	25.16 $\pm$ 0.03	46.32 $\pm$ 0.26	40.04 $\pm$ 0.09
BHyT	O	3.268	<b>3.254</b>	25.908	<b>0.385</b>	30.50 $\pm$ 0.16	62.42 $\pm$ 0.41	32.11 $\pm$ 0.10	<b>33.88</b> $\pm$ 0.73	50.15 $\pm$ 0.32	25.19 $\pm$ 0.02	<b>61.86</b> $\pm$ 0.17	<b>42.30</b> $\pm$ 0.13

We additionally examine the impact of the proposed variance approximation on model performance. Table 5 compares the exact variance calculation methods (RMSNorm, BHyT\*) against their approximate counterparts (RMSNorm-Approx, BHyT), following the same setup as Table 1. The results demonstrate that employing variance approximation yields significant computational benefits, improving training speed by approximately 10.1% for RMSNorm and 14.9% for BHyT\*. Crucially, this substantial gain in throughput comes with negligible degradation in pretraining loss and downstream accuracy, confirming that our approximation design effectively resolves computational bottlenecks without compromising the model’s representational capability.

## 5 CONCLUSION

We proposed Bounded Hyperbolic Tanh (BHyT) to reconcile the conflict between stability and efficiency in deep LLMs. By coupling explicit probabilistic bounding with a lightweight variance approximation, BHyT effectively neutralizes the ‘curse of depth’ without the computational overhead of repeated normalization. Validated by both rigorous theoretical bounds and extensive empirical results, our method offers a new paradigm for building deeper, more efficient foundation models. Beyond a mere architectural improvement, BHyT paves the way for scalable training regimes where computational efficiency does not come at the cost of training stability, serving as a robust foundation for next-generation large-scale architectures.

## REFERENCES

Jimmy Lei Ba, Jamie Ryan Kiros, and Geoffrey E Hinton. Layer normalization. *arXiv preprint arXiv:1607.06450*, 2016.

- Yonatan Bisk, Rowan Zellers, Jianfeng Gao, Yejin Choi, et al. Piqa: Reasoning about physical commonsense in natural language. In *Proceedings of the AAAI conference on artificial intelligence*, volume 34, pp. 7432–7439, 2020.
- Tom Brown, Benjamin Mann, Nick Ryder, Melanie Subbiah, Jared D Kaplan, Prafulla Dhariwal, Arvind Neelakantan, Pranav Shyam, Girish Sastry, Amanda Askell, et al. Language models are few-shot learners. *Advances in neural information processing systems*, 33:1877–1901, 2020.
- Christopher Clark, Kenton Lee, Ming-Wei Chang, Tom Kwiatkowski, Michael Collins, and Kristina Toutanova. BoolQ: Exploring the surprising difficulty of natural yes/no questions. In Jill Burstein, Christy Doran, and Thamar Solorio (eds.), *Proceedings of the 2019 Conference of the North American Chapter of the Association for Computational Linguistics: Human Language Technologies, Volume 1 (Long and Short Papers)*, pp. 2924–2936, Minneapolis, Minnesota, June 2019. Association for Computational Linguistics. doi: 10.18653/v1/N19-1300. URL <https://aclanthology.org/N19-1300/>.
- Peter Clark, Isaac Cowhey, Oren Etzioni, Tushar Khot, Ashish Sabharwal, Carissa Schoenick, and Oyvind Tafjord. Think you have solved question answering? try arc, the ai2 reasoning challenge. *arXiv preprint arXiv:1803.05457*, 2018.
- Tri Dao. Flashattention-2: Faster attention with better parallelism and work partitioning. *arXiv preprint arXiv:2307.08691*, 2023.
- Leo Gao, Jonathan Tow, Baber Abbasi, Stella Biderman, Sid Black, Anthony DiPofi, Charles Foster, Laurence Golding, Jeffrey Hsu, Alain Le Noac’h, Haonan Li, Kyle McDonell, Niklas Muenighoff, Chris Ociepa, Jason Phang, Laria Reynolds, Hailey Schoelkopf, Aviya Skowron, Lintang Sutawika, Eric Tang, Anish Thite, Ben Wang, Kevin Wang, and Andy Zou. The language model evaluation harness, 07 2024. URL <https://zenodo.org/records/12608602>.
- Dan Hendrycks, Collin Burns, Steven Basart, Andy Zou, Mantas Mazeika, Dawn Song, and Jacob Steinhardt. Measuring massive multitask language understanding. *arXiv preprint arXiv:2009.03300*, 2020.
- Jeonghoon Kim, Byeongchan Lee, Cheonbok Park, Yeontaek Oh, Beomjun Kim, Taehwan Yoo, Seongjin Shin, Dongyoon Han, Jinwoo Shin, and Kang Min Yoo. Peri-LN: Revisiting normalization layer in the transformer architecture. In *Forty-second International Conference on Machine Learning*, 2025. URL <https://openreview.net/forum?id=c1lS6wmXfO>.
- Michel Ledoux. *The Concentration of Measure Phenomenon*, volume 89 of *Mathematical Surveys and Monographs*. American Mathematical Society, Providence, RI, 2001.
- Todor Mihaylov, Peter Clark, Tushar Khot, and Ashish Sabharwal. Can a suit of armor conduct electricity? a new dataset for open book question answering. In *EMNLP*, 2018.
- Alec Radford, Jeffrey Wu, Rewon Child, David Luan, Dario Amodei, Ilya Sutskever, et al. Language models are unsupervised multitask learners. *OpenAI blog*, 1(8):9, 2019.
- Colin Raffel, Noam Shazeer, Adam Roberts, Katherine Lee, Sharan Narang, Michael Matena, Yanqi Zhou, Wei Li, and Peter J Liu. Exploring the limits of transfer learning with a unified text-to-text transformer. *Journal of machine learning research*, 21(140):1–67, 2020.
- Keisuke Sakaguchi, Ronan Le Bras, Chandra Bhagavatula, and Yejin Choi. Winogrande: An adversarial winograd schema challenge at scale. *Communications of the ACM*, 64(9):99–106, 2021.
- Noam Shazeer. Glu variants improve transformer. *arXiv preprint arXiv:2002.05202*, 2020.
- Wenfang Sun, Xinyuan Song, Pengxiang Li, Lu Yin, Yefeng Zheng, and Shiwei Liu. The curse of depth in large language models. *arXiv preprint arXiv:2502.05795*, 2025.
- Hugo Touvron, Thibaut Lavril, Gautier Izacard, Xavier Martinet, Marie-Anne Lachaux, Timothée Lacroix, Baptiste Rozière, Naman Goyal, Eric Hambro, Faisal Azhar, et al. Llama: Open and efficient foundation language models. *arXiv preprint arXiv:2302.13971*, 2023.

- Ashish Vaswani, Noam Shazeer, Niki Parmar, Jakob Uszkoreit, Llion Jones, Aidan N Gomez, Lukasz Kaiser, and Illia Polosukhin. Attention is all you need. *Advances in neural information processing systems*, 30, 2017.
- Ruibin Xiong, Yunchang Yang, Di He, Kai Zheng, Shuxin Zheng, Chen Xing, Huishuai Zhang, Yanyan Lan, Liwei Wang, and Tiejun Liu. On layer normalization in the transformer architecture. In *International conference on machine learning*, pp. 10524–10533. PMLR, 2020.
- Rowan Zellers, Ari Holtzman, Yonatan Bisk, Ali Farhadi, and Yejin Choi. Hellaswag: Can a machine really finish your sentence? *arXiv preprint arXiv:1905.07830*, 2019.
- Biao Zhang and Rico Sennrich. Root mean square layer normalization. *Advances in neural information processing systems*, 32, 2019.
- Yaowei Zheng, Richong Zhang, Junhao Zhang, Yanhan Ye, Zheyang Luo, Zhangchi Feng, and Yongqiang Ma. Llamafactory: Unified efficient fine-tuning of 100+ language models. In *Proceedings of the 62nd Annual Meeting of the Association for Computational Linguistics (Volume 3: System Demonstrations)*, Bangkok, Thailand, 2024. Association for Computational Linguistics. URL <http://arxiv.org/abs/2403.13372>.
- Chunting Zhou, Pengfei Liu, Puxin Xu, Srinivasan Iyer, Jiao Sun, Yuning Mao, Xuezhe Ma, Avia Efrat, Ping Yu, Lili Yu, et al. Lima: Less is more for alignment. *Advances in Neural Information Processing Systems*, 36:55006–55021, 2023.
- Jiachen Zhu, Xinlei Chen, Kaiming He, Yann LeCun, and Zhuang Liu. Transformers without normalization. In *Proceedings of the Computer Vision and Pattern Recognition Conference*, pp. 14901–14911, 2025.

## A STATEMENT ON THE USE OF LARGE LANGUAGE MODELS

LLMs were employed solely as a writing assistant to perform limited tasks such as grammar checking and improving readability. The core scientific aspects of this work, including the conception of ideas, development of methodology, theoretical and experimental studies, and drafting of the manuscript, were carried out entirely by the authors without contributions from the LLMs.

## B PROOFS OF THE THEOREMS

### B.1 PROOF OF PROPOSITION 3.1

**Proposition B.1** (Input scaling bound at the level  $p$ ). *Let  $x \in \mathbb{R}$  with  $\mathbb{E}[x] = \mu_x$  and  $\text{Var}(x) = s_x^2$ . Given a predefined bound  $\lambda > 0$  and target probability  $p \in (0, 1)$ , if  $\alpha = \frac{\lambda}{\kappa s_x + |\mu_x|}$ , then  $P(|\alpha x| \leq \lambda) \geq p$  for any distribution with finite variance, where  $\kappa := (1 - p)^{-1/2}$ .*

*Proof.* We aim to guarantee that the scaled variable  $\alpha x$  lies within the predefined bound  $[-\lambda, \lambda]$  with probability at least  $p$ , i.e.,

$$P(|\alpha x| \leq \lambda) \geq p.$$

This condition is equivalent to

$$P\left(|x| \leq \frac{\lambda}{|\alpha|}\right) \geq p.$$

By the triangle inequality, we have

$$|x| = |x - \mu_x + \mu_x| \leq |x - \mu_x| + |\mu_x|.$$

Therefore, the event  $\{x \mid |x - \mu_x| \leq \kappa s_x\}$  implies  $\{x \mid |x| \leq \kappa s_x + |\mu_x|\}$ , and hence

$$\{x \mid |x - \mu_x| \leq \kappa s_x\} \subseteq \{x \mid |x| \leq \kappa s_x + |\mu_x|\}. \quad (6)$$

If we choose  $\kappa$  such that

$$\kappa s_x + |\mu_x| \leq \frac{\lambda}{|\alpha|},$$

then, by the monotonicity of probability,

$$P\left(|x| \leq \frac{\lambda}{|\alpha|}\right) \geq P(|x - \mu_x| \leq \kappa s_x).$$

Applying Chebyshev's inequality,

$$P(|x - \mu_x| \leq \kappa s_x) \geq 1 - \frac{1}{\kappa^2}.$$

Setting  $\kappa := (1 - p)^{-1/2}$  yields

$$P\left(|x| \leq \frac{\lambda}{|\alpha|}\right) \geq p.$$

Solving  $\kappa s_x + |\mu_x| = \lambda/|\alpha|$  for  $\alpha$  gives

$$\alpha = \frac{\lambda}{\kappa s_x + |\mu_x|}.$$

□

### B.2 PROOF OF THEOREM 3.4

**Theorem 3.4** (Variance approximation of attention output). *Under Assumption 3.3, let  $h_{Attn} \in \mathbb{R}^d$  denote the output vector of the attention layer. The average coordinate-wise variance of the output, denoted by  $\tilde{s}_{h_{Attn}}^2 := \frac{1}{d} \sum_{k=1}^d \text{Var}((h_{Attn})_k)$ , is approximated as:*

$$\tilde{s}_{h_{Attn}}^2 \approx \frac{1}{Td} \|W_V W_O\|_F^2 \cdot \frac{\lambda_{Attn}^2}{\kappa^2}. \quad (4)$$

*Proof.* We aim to estimate the variance of the attention output to analyze signal propagation without computing the actual forward pass. Under Assumption 3.3, for a large sequence length  $T$ , the attention weights are approximately uniform. Consequently, the output vector  $h_{\text{Attn}}$  (viewed as a row vector) can be approximated as the average of the projected value vectors:

$$h_{\text{Attn}} \approx \frac{1}{T} \sum_{t=1}^T z_t W_V W_O,$$

where  $z_t$  is the activation of the  $t$ -th token after BHyT, and we let  $W = W_V W_O$ . Since the inputs and weights are zero-mean, the output  $h_{\text{Attn}}$  also has a zero-mean. Therefore, the variance of the  $k$ -th coordinate is  $\text{Var}((h_{\text{Attn}})_k) = \mathbb{E}[(h_{\text{Attn}})_k^2]$ . Substituting this into the definition of  $\tilde{s}_{h_{\text{Attn}}}^2$ , we can express the average variance using the trace of the covariance matrix:

$$\tilde{s}_{h_{\text{Attn}}}^2 = \frac{1}{d} \sum_{k=1}^d \mathbb{E}[(h_{\text{Attn}})_k^2] = \frac{1}{d} \mathbb{E}[\|h_{\text{Attn}}\|_2^2] = \frac{1}{d} \text{Tr}(\text{Cov}(h_{\text{Attn}})).$$

Since the token activations  $z_t$  are assumed to be independent and identically distributed, the covariance of the  $h_{\text{Attn}}$  is

$$\text{Cov}(h_{\text{Attn}}) \approx \text{Cov}\left(\frac{1}{T} \sum_{t=1}^T z_t W\right) = \frac{1}{T^2} \sum_{t=1}^T W^\top \text{Cov}(z_t) W.$$

According to Assumption 3.3, the input elements are i.i.d., and BHyT operates element-wise. Thus, the output coordinates of  $z_t$  remain uncorrelated, leading to a diagonal covariance matrix. With the sample variance given as approximately  $\lambda^2/\kappa^2$ , we have  $\text{Cov}(z_t) \approx \frac{\lambda_{\text{Attn}}^2}{\kappa^2} I_d$ . Substituting this into the trace expression yields:

$$\tilde{s}_{h_{\text{Attn}}}^2 \approx \frac{1}{d} \text{Tr}\left(\frac{1}{T^2} \sum_{t=1}^T W^\top \left(\frac{\lambda_{\text{Attn}}^2}{\kappa^2} I_d\right) W\right) = \frac{1}{d} \text{Tr}\left(\frac{1}{T} \frac{\lambda_{\text{Attn}}^2}{\kappa^2} W^\top W\right).$$

Finally, using the identity  $\text{Tr}(W^\top W) = \|W\|_F^2$ , we obtain the stated approximation:

$$\tilde{s}_{h_{\text{Attn}}}^2 \approx \frac{1}{Td} \|W_V W_O\|_F^2 \frac{\lambda_{\text{Attn}}^2}{\kappa^2}.$$

□

Strictly speaking, the normalization by  $s_x$  introduces weak dependencies between feature dimensions. However, for high-dimensional vectors (large  $d$ ), the impact of these dependencies on the covariance structure is negligible ( $O(1/d)$ ), allowing us to approximate  $\text{Cov}(z_t)$  as a diagonal matrix.

### B.3 APPROXIMATION OF THE VARIANCE OF THE MLP LAYER OUTPUT

**Theorem B.2** (Variance approximation of MLP layer output). *Let  $z \in \mathbb{R}^d$  be the input to the MLP sublayer with sample variance  $s_z^2$ , and let  $h_{\text{MLP}} \in \mathbb{R}^d$  be the output. The MLP consists of two linear transformations parameterized by  $W_1 \in \mathbb{R}^{d \times d_m}$  and  $W_2 \in \mathbb{R}^{d_m \times d}$ , separated by an element-wise activation function  $\phi(\cdot)$ . We assume that the activation function scales the covariance of its input by a factor  $\tau$  (i.e.,  $\text{Cov}(\phi(u)) \approx \tau \text{Cov}(u)$ ). The average sample variance of the MLP output, denoted by  $\tilde{s}_{h_{\text{MLP}}}^2$ , is approximated as:*

$$\tilde{s}_{h_{\text{MLP}}}^2 \approx \tau \frac{s_z^2}{d} \|W_1 W_2\|_F^2.$$

*Proof.* We analyze the propagation of variance through the MLP block defined by  $h_{\text{MLP}} = \phi(zW_1)W_2$ . Let  $u = zW_1$  be the pre-activation vector and  $v = \phi(u)$  be the post-activation vector. Similar to the definition in Theorem 3.4, the average sample variance of the output is given by the trace of its covariance matrix:

$$\tilde{s}_{h_{\text{MLP}}}^2 = \frac{1}{d} \text{Tr}(\text{Cov}(h_{\text{MLP}})).$$

We expand the covariance of the output with respect to the second linear layer as:

$$\text{Cov}(h_{\text{MLP}}) = \text{Cov}(vW_2) = W_2^\top \text{Cov}(v)W_2.$$

Under the assumption that the activation function  $\phi$  essentially acts as a scaling factor  $\tau$  on the covariance matrix (which holds exactly for linear activations or as a linear approximation for nonlinear ones), we substitute  $\text{Cov}(v) \approx \tau \text{Cov}(u)$ :

$$\text{Cov}(h_{\text{MLP}}) \approx W_2^\top (\tau \text{Cov}(u))W_2 = \tau W_2^\top \text{Cov}(zW_1)W_2.$$

Further expanding  $\text{Cov}(u) = \text{Cov}(zW_1) = W_1^\top \text{Cov}(z)W_1$ , we obtain:

$$\text{Cov}(h_{\text{MLP}}) \approx \tau W_2^\top (W_1^\top \text{Cov}(z)W_1)W_2 = \tau (W_1W_2)^\top \text{Cov}(z)(W_1W_2).$$

Assuming the input  $z$  consists of uncorrelated elements with uniform variance  $s_z^2$  (consistent with the output of BHyT where  $s_z^2 \approx \lambda^2/\kappa^2$ ), the covariance of the input is  $\text{Cov}(z) = s_z^2 I_d$ . Substituting this into the expression gives:

$$\text{Cov}(h_{\text{MLP}}) \approx \tau s_z^2 (W_1W_2)^\top (W_1W_2).$$

Finally, taking the trace to find the average sample variance:

$$\tilde{s}_{h_{\text{MLP}}}^2 = \frac{1}{d} \text{Tr}(\tau s_z^2 (W_1W_2)^\top (W_1W_2)) = \tau \frac{s_z^2}{d} \text{Tr}((W_1W_2)^\top (W_1W_2)).$$

By the definition of the Frobenius norm,  $\text{Tr}(A^\top A) = \|A\|_F^2$ , which leads to the final approximation:

$$\tilde{s}_{h_{\text{MLP}}}^2 \approx \tau \frac{s_z^2}{d} \|W_1W_2\|_F^2.$$

□

While Llama architectures employ SwiGLU (Shazeer, 2020) variants involving three matrices (gate, up, down), for theoretical tractability, we analyze the standard MLP formulation parameterized by  $W_1$  and  $W_2$ . We assume this variance propagation logic generalizes to Gated units by treating the gating mechanism as part of the effective activation scaling factor  $\tau$ .

## B.4 PROOF OF THEOREM 3.5

### B.4.1 VARIANCE BOUND FOR BHyT

**Lemma B.3** (Variance bound for tanh in BHyT). *Let  $x$  be a scalar random variable with a probability density function symmetric about zero, such that  $\mathbb{E}[x] = 0$  and  $\text{Var}(x) = s_x^2$ . Define the scaling factor  $\alpha = \frac{\lambda}{\kappa s_x}$  for hyperparameters  $\lambda, \kappa > 0$ . Assuming the bound  $|\alpha x| \leq \lambda$  holds (or conditioning on this event), the variance of the activation satisfies:*

$$\left(\frac{\tanh(\lambda)}{\lambda}\right)^2 \frac{\lambda^2}{\kappa^2} \leq \text{Var}(\tanh(\alpha x)) \leq \frac{\lambda^2}{\kappa^2}.$$

*Proof.* First, we establish point-wise inequalities for the function  $h(t) = \tanh(t)$  on the interval  $[-\lambda, \lambda]$ .

Upper Bound: For any real number  $t$ , it is a standard property that  $|\tanh(t)| \leq |t|$ . Squaring both sides gives:

$$\tanh^2(t) \leq t^2.$$

Substituting  $t = \alpha x$ , we obtain  $\tanh^2(\alpha x) \leq (\alpha x)^2$ . Taking the expectation on both sides:

$$\mathbb{E}[\tanh^2(\alpha x)] \leq \mathbb{E}[(\alpha x)^2] = \alpha^2 \mathbb{E}[x^2] = \alpha^2 s_x^2.$$

Substituting  $\alpha = \frac{\lambda}{\kappa s_x}$ , we get  $\alpha^2 s_x^2 = \left(\frac{\lambda}{\kappa s_x}\right)^2 s_x^2 = \frac{\lambda^2}{\kappa^2}$ . Since  $\mathbb{E}[x] = 0$  and the distribution is symmetric,  $\mathbb{E}[\tanh(\alpha x)] = 0$ , implying  $\text{Var}(\tanh(\alpha x)) = \mathbb{E}[\tanh^2(\alpha x)]$ . Thus the upper bound of  $\text{Var}(\tanh(\alpha x))$  is

$$\text{Var}(\tanh(\alpha x)) \leq \frac{\lambda^2}{\kappa^2}.$$

Lower Bound: Consider  $t \in [0, \lambda]$ . Since  $h(t) = \tanh(t)$  is concave on  $[0, \infty)$  and  $h(0) = 0$ , the secant line connecting  $(0, 0)$  and  $(\lambda, \tanh(\lambda))$  lies below the graph of  $h(t)$  for  $t \in [0, \lambda]$ . The equation of this line is  $y = \frac{\tanh(\lambda)}{\lambda}t$ . Therefore:

$$\tanh(t) \geq \frac{\tanh(\lambda)}{\lambda}t \quad \text{for } t \in [0, \lambda].$$

By the odd symmetry of  $\tanh(t)$ , for  $t \in [-\lambda, 0]$ , we have  $\tanh(t) \leq \frac{\tanh(\lambda)}{\lambda}t$  (since both sides are negative). Squaring both cases yields the same inequality for all  $t \in [-\lambda, \lambda]$ :

$$\tanh^2(t) \geq \left(\frac{\tanh(\lambda)}{\lambda}\right)^2 t^2.$$

Substituting  $t = \alpha x$  and taking the expectation (under the assumption  $|\alpha x| \leq \lambda$ ):

$$\mathbb{E}[\tanh^2(\alpha x)] \geq \left(\frac{\tanh(\lambda)}{\lambda}\right)^2 \mathbb{E}[(\alpha x)^2] = \left(\frac{\tanh(\lambda)}{\lambda}\right)^2 \frac{\lambda^2}{\kappa^2}.$$

□

#### B.4.2 VARIANCE RECURSION WITH RESIDUAL CONNECTIONS

We next derive the variance recursion for a generic residual block of the form

$$x'_\ell = x_\ell + h_\ell, \quad x_{\ell+1} = x'_\ell + g_\ell,$$

where  $h_\ell = \text{Attn}(f(x_\ell))$  and  $g_\ell = \text{MLP}(f(x'_\ell))$ . Here,  $f(\cdot)$  denotes a normalization layer (e.g., RMSNorm, BHyT, etc.).

**Lemma B.4** (Generic variance recursion). *Let  $\tilde{s}_{x_\ell}^2$  and  $\tilde{s}_{x'_\ell}^2$  denote the average sample variances of the residual stream before and after the attention sublayer at layer  $\ell$ . Based on the approximations in Theorems 3.4 and B.2, we define the structural amplification factors as:*

$$C_{\text{Attn}} := \frac{1}{T_d} \|W_V W_O\|_F^2, \quad C_{\text{MLP}} := \frac{\tau}{d} \|W_1 W_2\|_F^2.$$

Let  $\tilde{s}_{f(x_\ell)}^2$  and  $\tilde{s}_{f(x'_\ell)}^2$  be the variances of the normalization layer outputs. Assuming linear correlations parameterized by coefficients  $\rho_1$  and  $\rho_2$ , the variances satisfy the recursion:

$$\begin{aligned} \tilde{s}_{x'_\ell}^2 &= \tilde{s}_{x_\ell}^2 + C_{\text{Attn}} \tilde{s}_{f(x_\ell)}^2 + 2\rho_1 \tilde{s}_{x_\ell} \sqrt{C_{\text{Attn}} \tilde{s}_{f(x_\ell)}^2}, \\ \tilde{s}_{x_{\ell+1}}^2 &= \tilde{s}_{x'_\ell}^2 + C_{\text{MLP}} \tilde{s}_{f(x'_\ell)}^2 + 2\rho_2 \tilde{s}_{x'_\ell} \sqrt{C_{\text{MLP}} \tilde{s}_{f(x'_\ell)}^2}. \end{aligned}$$

*Proof.* We analyze the variance accumulation through the residual connections. For the attention sublayer, the residual update is  $x'_\ell = x_\ell + h_\ell$ . By the properties of variance, we have:

$$\text{Var}(x'_\ell) = \text{Var}(x_\ell) + \text{Var}(h_\ell) + 2\text{Cov}(x_\ell, h_\ell).$$

Using the average sample variance notation  $\tilde{s}^2$ , and applying the result from Theorem 3.4, the variance of the attention output is approximated by the product of the structural factor and the input variance:  $\tilde{s}_{h_\ell}^2 \approx C_{\text{Attn}} \tilde{s}_{f(x_\ell)}^2$ . For the covariance term, we introduce the correlation coefficient  $\rho_1$  between the residual stream  $x_\ell$  and the attention sublayer output  $h_\ell$ , such that:

$$\text{Cov}(x_\ell, h_\ell) = \rho_1 \sqrt{\text{Var}(x_\ell)} \sqrt{\text{Var}(h_\ell)} = \rho_1 \tilde{s}_{x_\ell} \tilde{s}_{h_\ell} \approx \rho_1 \tilde{s}_{x_\ell} \sqrt{C_{\text{Attn}} \tilde{s}_{f(x_\ell)}^2}.$$

Substituting these terms back into the variance equation yields the first recursion formula. The derivation for the MLP sublayer follows strictly analogous steps. Starting from  $x_{\ell+1} = x'_\ell + g_\ell$ , we expand the variance as  $\tilde{s}_{x_{\ell+1}}^2 = \tilde{s}_{x'_\ell}^2 + \tilde{s}_{g_\ell}^2 + 2\text{Cov}(x'_\ell, g_\ell)$ . Invoking Theorem B.2, the MLP output variance is  $\tilde{s}_{g_\ell}^2 \approx C_{\text{MLP}} \tilde{s}_{f(x'_\ell)}^2$ . Defining  $\rho_2$  as the correlation coefficient between  $x'_\ell$  and  $g_\ell$ , the covariance is modeled as  $\rho_2 \tilde{s}_{x'_\ell} \sqrt{C_{\text{MLP}} \tilde{s}_{f(x'_\ell)}^2}$ . □

### B.4.3 SPECIALIZATION TO RMSNORM, LNS AND BHyT

In this section, we instantiate the generic variance recursion from the assumptions and results of Theorems 3.4 and B.2, for three concrete choices of  $f(\cdot)$ : RMSNorm, LNS (Sun et al., 2025), and BHyT. We follow the derivation in Appendix B.4.2.

**Notation.** We denote by

$$s_{x_\ell}^2 = \text{Var}(x_\ell), \quad s_{x'_\ell}^2 = \text{Var}(x'_\ell), \quad s_{f(x_\ell)}^2 = \text{Var}(f(x_\ell)), \quad s_{f(x'_\ell)}^2 = \text{Var}(f(x'_\ell)).$$

The output variances of the attention and MLP sublayers are  $s_{\text{Attn},\ell}^2 = \text{Var}(\text{Attn}(f(x_\ell)))$  and  $s_{\text{MLP},\ell}^2 = \text{Var}(\text{MLP}(f(x'_\ell)))$ , respectively.

### B.4.4 VARIANCE RECURSION AND PRODUCT FORM

To simplify the recursion, we define the normalized variance gains  $\pi_{\text{Attn},\ell}$  and  $\pi_{\text{MLP},\ell}$ , which represent the relative variance contribution of each sublayer scaled by the structural constants  $C_{\text{Attn}}$  and  $C_{\text{MLP}}$ :

$$\pi_{\text{Attn},\ell} := \frac{C_{\text{Attn}} \tilde{s}_{f(x_\ell)}^2}{\tilde{s}_{x_\ell}^2}, \quad \pi_{\text{MLP},\ell} := \frac{C_{\text{MLP}} \tilde{s}_{f(x'_\ell)}^2}{\tilde{s}_{x'_\ell}^2}.$$

We also define the scalar amplification function  $\delta(\rho, u)$  as:

$$\delta(\rho, \pi) := 1 + \pi + 2\rho\sqrt{\pi}.$$

Using Lemma B.4, the layer-wise variance amplification ratios can be written compactly as:

$$\begin{aligned} \frac{\tilde{s}_{x'_\ell}^2}{\tilde{s}_{x_\ell}^2} &= 1 + \frac{C_{\text{Attn}} \tilde{s}_{f(x_\ell)}^2}{\tilde{s}_{x_\ell}^2} + 2\rho_1 \sqrt{\frac{C_{\text{Attn}} \tilde{s}_{f(x_\ell)}^2}{\tilde{s}_{x_\ell}^2}} = \delta(\rho_1, \pi_{\text{Attn},\ell}), \\ \frac{\tilde{s}_{x_{\ell+1}}^2}{\tilde{s}_{x'_\ell}^2} &= 1 + \frac{C_{\text{MLP}} \tilde{s}_{f(x'_\ell)}^2}{\tilde{s}_{x'_\ell}^2} + 2\rho_2 \sqrt{\frac{C_{\text{MLP}} \tilde{s}_{f(x'_\ell)}^2}{\tilde{s}_{x'_\ell}^2}} = \delta(\rho_2, \pi_{\text{MLP},\ell}). \end{aligned}$$

Combining the amplification factors for both sublayers, the total variance growth for a single block at layer  $\ell$  is:

$$\frac{\tilde{s}_{x_{\ell+1}}^2}{\tilde{s}_{x_\ell}^2} = \delta(\rho_1, \pi_{\text{Attn},\ell}) \cdot \delta(\rho_2, \pi_{\text{MLP},\ell}).$$

Iterating this relation from layer  $\ell = 1$  to  $L - 1$ , we obtain the closed-form expression for the variance at the final layer  $L$ :

$$\tilde{s}_{x_L}^2 = \tilde{s}_{x_1}^2 \prod_{\ell=1}^{L-1} \delta(\rho_1, \pi_{\text{Attn},\ell}) \cdot \delta(\rho_2, \pi_{\text{MLP},\ell}).$$

This product form allows us to analyze the signal propagation behavior by simply substituting the specific normalized gains  $\pi$  corresponding to each normalization method (RMSNorm, LNS, and BHyT).

**Lemma B.5** (Depth-wise variance under RMSNorm). *Let  $f(x)$  be RMSNorm applied coordinate-wise to a  $d$ -dimensional vector  $x$ , defined by learnable scales  $\gamma \in \mathbb{R}^d$ . Let  $\tilde{s}_{x_\ell}^2$  and  $\tilde{s}_{x'_\ell}^2$  denote the average sample variances of the residual stream before and after the attention sublayer at layer  $\ell$ . We define the average squared scale as  $\gamma^2 = \frac{1}{d} \sum_{i=1}^d \gamma_i^2$ . Using the structural constants  $C_{\text{Attn}}$  and  $C_{\text{MLP}}$  defined in Lemma B.4, we define the normalized variance gains for RMSNorm as:*

$$\pi_{\text{Attn},\ell}^{\text{RMS}} := \frac{C_{\text{Attn}} \overline{\gamma_{\text{Attn}}^2}}{\tilde{s}_{x_\ell}^2}, \quad \pi_{\text{MLP},\ell}^{\text{RMS}} := \frac{C_{\text{MLP}} \overline{\gamma_{\text{MLP}}^2}}{\tilde{s}_{x'_\ell}^2}.$$

Let  $\delta(\rho, \pi) = 1 + \pi + 2\rho\sqrt{\pi}$  be the scalar amplification function. Then, the depth-wise variance accumulation under RMSNorm satisfies:

$$\tilde{s}_{x_L}^2 = \tilde{s}_{x_1}^2 \prod_{\ell=1}^{L-1} \delta(\rho_1, \pi_{\text{Attn},\ell}^{\text{RMS}}) \delta(\rho_2, \pi_{\text{MLP},\ell}^{\text{RMS}}).$$

*Proof.* We first determine the variance of the RMSNorm output. For a vector  $x$  with zero-mean, RMSNorm is defined as  $\text{RMSNorm}(x) = \gamma \odot \frac{x}{\sqrt{\frac{1}{d} \sum_{j=1}^d x_j^2}}$ . Squaring and taking the expectation,

and utilizing the symmetry of the isotropic input distribution (where  $\mathbb{E}[\frac{x_i^2}{\frac{1}{d} \sum_{j=1}^d x_j^2}] = 1$ ), we obtain:

$$\mathbb{E}[\text{RMSNorm}(x)_i^2] = \gamma_i^2 \cdot \mathbb{E}\left[\frac{x_i^2}{\frac{1}{d} \sum_{j=1}^d x_j^2}\right] = \gamma_i^2.$$

Thus, the average sample variance of the output is independent of the input variance magnitude and is determined solely by the scale parameters:

$$\tilde{s}_{f(x)}^2 = \frac{1}{d} \sum_{i=1}^d \gamma_i^2 = \overline{\gamma^2}.$$

Consequently, at any layer  $\ell$ , the variances of the normalization outputs feeding into the Attention and MLP blocks are identical:  $\tilde{s}_{f(x_\ell)}^2 = \overline{\gamma_{\text{Attn}}^2}$  and  $\tilde{s}_{f(x'_\ell)}^2 = \overline{\gamma_{\text{MLP}}^2}$ . Substituting these fixed variance terms into the definition of the normalized variance gains (from Lemma B.4) yields the specific forms for RMSNorm:

$$\pi_{\text{Attn},\ell}^{\text{RMS}} = \frac{C_{\text{Attn}} \tilde{s}_{f(x_\ell)}^2}{\tilde{s}_{x_\ell}^2} = \frac{C_{\text{Attn}} \overline{\gamma_{\text{Attn}}^2}}{\tilde{s}_{x_\ell}^2}, \quad \pi_{\text{MLP},\ell}^{\text{RMS}} = \frac{C_{\text{MLP}} \tilde{s}_{f(x'_\ell)}^2}{\tilde{s}_{x'_\ell}^2} = \frac{C_{\text{MLP}} \overline{\gamma_{\text{MLP}}^2}}{\tilde{s}_{x'_\ell}^2}.$$

□

**Lemma B.6** (Depth-wise variance under LNS). *Let  $f(x)$  be the LNS (Sun et al., 2025) operation, defined as RMSNorm followed by a depth-dependent scalar  $1/\sqrt{\ell}$  at layer  $\ell$ . Using the same notation as in Lemma B.5, the normalized variance gains for LNS are given by:*

$$\pi_{\text{Attn},\ell}^{\text{LNS}} \approx \frac{C_{\text{Attn}} \overline{\gamma_{\text{Attn}}^2}}{\ell \cdot \tilde{s}_{x_\ell}^2}, \quad \pi_{\text{MLP},\ell}^{\text{LNS}} \approx \frac{C_{\text{MLP}} \overline{\gamma_{\text{MLP}}^2}}{\ell \cdot \tilde{s}_{x'_\ell}^2}.$$

Consequently, the depth-wise variance accumulation under LNS satisfies:

$$\tilde{s}_{x_L}^2 = \tilde{s}_{x_1}^2 \prod_{\ell=1}^{L-1} \delta(\rho_1, \pi_{\text{Attn},\ell}^{\text{LNS}}) \delta(\rho_2, \pi_{\text{MLP},\ell}^{\text{LNS}}).$$

*Proof.* By Lemma B.5, the standard RMSNorm operation produces an output with average sample variance  $\tilde{s}_{\text{RMS}(x)}^2 = \overline{\gamma^2}$ , which is independent of the input variance. LNS introduces an additional scalar multiplication by  $1/\sqrt{\ell}$  after RMSNorm. Since variance scales quadratically with the multiplier, the variance of the LNS output at layer  $\ell$  becomes:

$$\tilde{s}_{f(x_\ell)}^2 = \text{Var}\left(\frac{1}{\sqrt{\ell}} \text{RMSNorm}(x_\ell)\right) = \frac{1}{\ell} \tilde{s}_{\text{RMS}(x_\ell)}^2 = \frac{\overline{\gamma^2}}{\ell}.$$

Substituting this result into the definition of the normalized variance gain  $\pi_{\text{Attn},\ell} = C_{\text{Attn}} \tilde{s}_{f(x_\ell)}^2 / \tilde{s}_{x_\ell}^2$ , we obtain:

$$\pi_{\text{Attn},\ell}^{\text{LNS}} = \frac{C_{\text{Attn}} (\overline{\gamma^2} / \ell)}{\tilde{s}_{x_\ell}^2} = \frac{C_{\text{Attn}} \overline{\gamma^2}}{\ell \cdot \tilde{s}_{x_\ell}^2}.$$

The derivation for the MLP sublayer term  $\pi_{\text{MLP},\ell}^{\text{LNS}}$  follows identically. □

**Lemma B.7** (Depth-wise variance bounds under BHyT). *Let  $f(x)$  be the BHyT, parameterized by hyperparameters  $(\lambda, \kappa)$  and a learnable scale vector  $\gamma$ . Let  $\overline{\gamma^2}$  be the average squared of  $\gamma$ . Based on the variance bounds derived in Lemma B.3, we define the lower and upper bound approximations for the normalized variance gains at layer  $\ell$  as:*

$$\pi_{\text{Attn},\ell}^{\text{BHyT,low}} := \frac{C_{\text{Attn}} \overline{\gamma^2}}{\tilde{s}_{x_\ell}^2} \cdot \left(\frac{\tanh(\lambda_{\text{Attn}})}{\lambda_{\text{Attn}}}\right)^2 \cdot \frac{\lambda_{\text{Attn}}^2}{\kappa^2}, \quad \pi_{\text{Attn},\ell}^{\text{BHyT,up}} := \frac{C_{\text{Attn}} \overline{\gamma^2}}{\tilde{s}_{x_\ell}^2} \cdot \frac{\lambda_{\text{Attn}}^2}{\kappa^2}.$$

Analogous definitions apply for  $\pi_{MLP,\ell}^{BHyT,low}$  and  $\pi_{MLP,\ell}^{BHyT,up}$  by substituting the appropriate structural constant  $C_{MLP}$  and input variance  $\tilde{s}_{x_\ell}^2$ . Using the scalar amplification function  $\delta(\rho, \pi) = 1 + \pi + 2\rho\sqrt{\pi}$ , the depth-wise variance accumulation under BHyT satisfies the following two-sided bounds:

$$\tilde{s}_{x_1}^2 \prod_{\ell=1}^{L-1} \delta(\rho_1, \pi_{Attn,\ell}^{BHyT,low}) \delta(\rho_2, \pi_{MLP,\ell}^{BHyT,low}) \leq \tilde{s}_{x_L}^2 \leq \tilde{s}_{x_1}^2 \prod_{\ell=1}^{L-1} \delta(\rho_1, \pi_{Attn,\ell}^{BHyT,up}) \delta(\rho_2, \pi_{MLP,\ell}^{BHyT,up}).$$

*Proof.* We start by examining the variance of the BHyT output. BHyT is defined as  $f(x) = \gamma \odot \tanh(\frac{\lambda}{\kappa s_x} x)$ . According to Lemma B.3, the variance of the tanh component, denoted as  $z = \tanh(\frac{\lambda}{\kappa s_x} x)$ , is bounded by:

$$\left( \frac{\tanh(\lambda)}{\lambda} \right)^2 \frac{\lambda^2}{\kappa^2} \leq \text{Var}(z) \leq \frac{\lambda^2}{\kappa^2}.$$

Since the learnable scale  $\gamma$  acts element-wise, the average sample variance of the BHyT output  $\tilde{s}_{f(x)}^2$  is the product of the average squared scale  $\overline{\gamma^2}$  and the variance of the tanh activation. Therefore, the output variance at layer  $\ell$  is bounded by:

$$\overline{\gamma^2} \left( \frac{\tanh(\lambda)}{\lambda} \right)^2 \frac{\lambda^2}{\kappa^2} \leq \tilde{s}_{f(x_\ell)}^2 \leq \overline{\gamma^2} \frac{\lambda^2}{\kappa^2}.$$

Substituting these inequalities into the definition of the normalized variance gain  $\pi_{Attn,\ell} = C_{Attn} \tilde{s}_{f(x_\ell)}^2 / \tilde{s}_{x_\ell}^2$  yields the definitions for  $\pi_{Attn,\ell}^{BHyT,low}$  and  $\pi_{Attn,\ell}^{BHyT,up}$  stated in the Lemma B.7. Crucially, the scalar amplification function  $\delta(\rho, \pi) = 1 + \pi + 2\rho\sqrt{\pi}$  is monotonically increasing with respect to  $\pi$  for  $\pi > 0$  and  $\rho \geq 0$ . This monotonicity allows us to propagate the inequalities through the product-recursive form derived in Appendix B.4.4. specifically:

$$\delta(\rho_1, \pi_{Attn,\ell}^{BHyT,low}) \leq \delta(\rho_1, \pi_{Attn,\ell}) \leq \delta(\rho_1, \pi_{Attn,\ell}^{BHyT,up}).$$

Applying this relationship to both the Attention and MLP sublayers across all layers  $\ell = 1, \dots, L-1$  proves the stated lower and upper bounds for the final depth-wise variance  $\tilde{s}_{x_L}^2$ .  $\square$

#### B.4.5 PROOF OF THEOREM 3.5

**Theorem 3.5** (Finite-depth variance bound of BHyT). *For a network of depth  $L$ , if the BHyT hyperparameters satisfy  $\frac{\lambda}{\kappa} < \frac{1}{\sqrt{L}}$ , then the output variance of BHyT is strictly smaller than that of LNS (Sun et al., 2025) for every layer  $\ell$  up to depth  $L$  (i.e., for all  $1 \leq \ell \leq L$ ):*

$$\tilde{s}_{x_\ell}^{BHyT} < \tilde{s}_{x_\ell}^{LNS}, \quad \forall \ell \in \{1, \dots, L\}. \quad (5)$$

*Proof.* To compare the output variances of BHyT and LNS, we examine their respective layer-wise variance amplification factors derived in Lemma B.6 and Lemma B.7. Recall the recursive product form:

$$\tilde{s}_{x_L}^2 = \tilde{s}_{x_1}^2 \prod_{\ell=1}^{L-1} \delta(\rho_1, \pi_{Attn,\ell}) \delta(\rho_2, \pi_{MLP,\ell}).$$

Since the scalar amplification function  $\delta(\rho, \pi) = 1 + \pi + 2\rho\sqrt{\pi}$  is monotonically increasing with respect to  $\pi$  for  $\pi > 0$  and  $\rho \geq 0$ , it suffices to compare the normalized variance gain terms  $\pi$  at each layer  $\ell$ . From Lemma B.6, the variance gain for LNS at layer  $\ell$  scales as:

$$\pi_{Attn,\ell}^{LNS} = \frac{C_{Attn} \overline{\gamma_{Attn}^2}}{\ell \cdot \tilde{s}_{x_\ell}^2}, \quad \pi_{MLP,\ell}^{LNS} = \frac{C_{MLP} \overline{\gamma_{MLP}^2}}{\ell \cdot \tilde{s}_{x'_\ell}^2}.$$

From Lemma B.7, the upper bound of the variance gain for BHyT at layer  $\ell$  is determined by:

$$\pi_{Attn,\ell}^{BHyT,up} = \frac{C_{Attn} \overline{\gamma_{Attn}^2} \left( \frac{\lambda_{Attn}^2}{\kappa^2} \right)}{\tilde{s}_{x_\ell}^2}, \quad \pi_{MLP,\ell}^{BHyT,up} = \frac{C_{MLP} \overline{\gamma_{MLP}^2} \left( \frac{\lambda_{MLP}^2}{\kappa^2} \right)}{\tilde{s}_{x'_\ell}^2}.$$

For the output variance of BHyT to be strictly smaller than that of LNS, the amplification factor of BHyT must be smaller than that of LNS at each layer. Comparing the Attention terms (the MLP terms follow analogously), we require:

$$\delta(\rho_1, \pi_{\text{Attn}, \ell}^{\text{BHyT, up}}) < \delta(\rho_1, \pi_{\text{Attn}, \ell}^{\text{LNS}}).$$

Due to the monotonicity of  $\delta$ , this inequality holds if and only if  $\pi_{\text{Attn}, \ell}^{\text{BHyT, up}} < \pi_{\text{Attn}, \ell}^{\text{LNS}}$ . Substituting the explicit forms into the comparison:

$$\frac{C_{\text{Attn}} \overline{\gamma_{\text{Attn}}^2} \frac{\lambda_{\text{Attn}}^2}{\kappa^2}}{\tilde{s}_{x_\ell}^2} < \frac{C_{\text{Attn}} \overline{\gamma_{\text{Attn}}^2}}{\ell \cdot \tilde{s}_{x_\ell}^2}.$$

Canceling the common positive terms  $(C_{\text{Attn}}, \overline{\gamma_{\text{Attn}}^2}, \tilde{s}_{x_\ell}^2)$ , we obtain the condition for the scaling factors:

$$\frac{\lambda_{\text{Attn}}^2}{\kappa^2} < \frac{1}{\ell}.$$

Taking the square root implies  $\frac{\lambda_{\text{Attn}}}{\kappa} < \frac{1}{\sqrt{\ell}}$ . The term  $\frac{1}{\sqrt{\ell}}$  is a decreasing function of  $\ell$ . Therefore, satisfying this condition for the maximum depth  $L$  (i.e.,  $\frac{\lambda_{\text{Attn}}}{\kappa} < \frac{1}{\sqrt{L}}$ ) ensures that it holds for all shallower layers  $\ell < L$ . Consequently, if this condition is met, the per-layer variance multiplier of BHyT is strictly smaller than that of LNS for all layers, leading to the final inequality:

$$\tilde{s}_{x_L}^{\text{BHyT}} < \tilde{s}_{x_L}^{\text{LNS}}.$$

□

## C HYPERPARAMETER SEARCH AND EXPERIMENTAL SETUP

**Hyperparameter Search Protocol** We perform hyperparameter tuning within a shared sweep range to ensure a fair comparison across all normalization methods. For each method, we identify the optimal configuration by selecting the hyperparameters that achieve the lowest evaluation loss after the Llama-1B model completes 20K pretraining steps. This selected configuration is then used for the full pretraining run and subsequently for supervised fine-tuning (SFT).

### C.1 HYPERPARAMETERS FOR PRETRAINING

#### Common sweep ranges

- **Learning rate (LR):**  $\{1\text{e-}4, 3\text{e-}4, 5\text{e-}4, 1\text{e-}3, 3\text{e-}3\}$
- **Weight decay (WD):**  $\{0.0, 0.1\}$
- **Min LR ratio:**  $\{1\text{e-}1, 1\text{e-}2\}$
- **Warmup ratio:**  $\{5\text{e-}2, 1\text{e-}1\}$

#### Method-specific sweep ranges

- **BHyT:** initial values of  $\lambda$ :  $\{1.0, 2.0, 3.0, 4.0, 5.0\}$
- **DyT:** learnable tanh-scaling parameter initialized using recommended values from the DyT (Zhu et al., 2025): the learnable tanh-scaling parameter is initialized following the values recommended in the original paper (Zhu et al., 2025): for Llama-1B, we set the scalars to 1.0 (before Attention), 0.5 (before MLP), and 0.5 (last layer), while for Llama-3B we use 0.2, 0.05, and 0.05, respectively.

### C.2 SFT HYPERPARAMETER SWEEP

- **Learning rate (LR):**  $\{1\text{e-}7, 5\text{e-}7, 1\text{e-}6, 1\text{e-}5, 5\text{e-}5, 1\text{e-}4\}$
- **Weight decay (WD):**  $\{0.0, 0.1\}$
- **Min LR ratio:**  $\{1\text{e-}1, 1\text{e-}2, 1\text{e-}3\}$
- **Warmup ratio:**  $\{3\text{e-}2, 5\text{e-}2, 1\text{e-}1\}$

### C.3 FINAL HYPERPARAMETER CONFIGURATIONS

- RMSNorm: {LR:  $3e-4$ , WD: 0.1, Min LR ratio:  $1e-1$ , Warmup ratio:  $1e-1$ }
- Peri-LN: {LR:  $3e-4$ , WD: 0.1, Min LR ratio:  $1e-1$ , Warmup ratio:  $1e-1$ }
- LNS: {LR:  $5e-4$ , WD: 0.1, Min LR ratio:  $1e-1$ , Warmup ratio:  $5e-2$ }
- DyT: {LR:  $1e-4$ , WD: 0.1, Min LR ratio:  $1e-1$ , Warmup ratio:  $1e-1$ }
- BHyT: {LR:  $5e-4$ , WD: 0.1, Min LR ratio:  $1e-2$ , Warmup ratio:  $1e-1$ ,  $\lambda$  values:  $BHyT_{Attm}: 2.0$ ,  $BHyT_{MLP}: 1.0$ }

### C.4 HARDWARE AND SYSTEM CONFIGURATION

- **Pretrain and SFT framework:** Llama-Factory (Zheng et al., 2024)
- **Llama-1B GPU:** RTX A6000
- **Llama-3B GPU:** RTX PRO 6000 Blackwell
- **Parallel computation:** For efficient parallel computation, we use FlashAttention-2 (Dao, 2023)
- **Distributed training:** DeepSpeed ZeRO-2

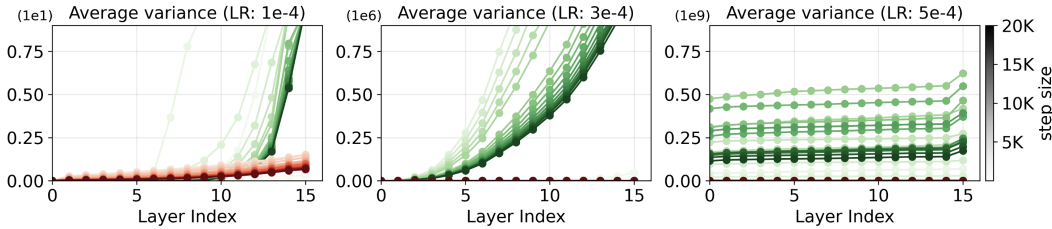
## D ADDITIONAL EXPERIMENTAL RESULTS

### D.1 TIME TO TARGET LOSS ANALYSIS

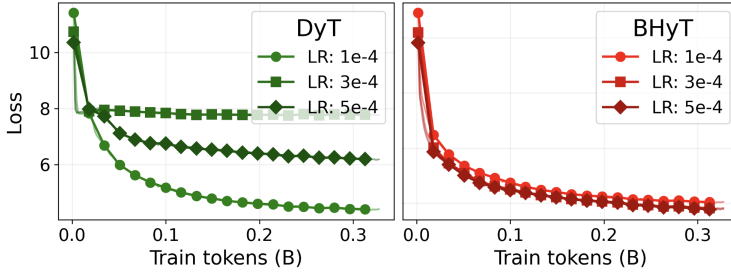
Table 6: Time-to-target-loss comparison for Llama-1B and Llama-3B. Each method is evaluated at the loss value that BHyT reaches roughly 5K steps before completing pretraining. Most baselines reach this loss only much later or fail to reach it within the training budget.

Llama-1B											
Method	PT Train Loss	Wall time (hour)	Checkpoint Step	Arc-e	PIQA	Hellaswag	OpenBookQA	Winogrande	MMLU	BoolQ	Avg.
RMSNorm	3.282	39.35	49K	$30.97_{\pm 0.20}$	$62.89_{\pm 0.74}$	$32.77_{\pm 0.09}$	$32.32_{\pm 0.94}$	<b>50.54</b> $_{\pm 0.48}$	<b>25.70</b> $_{\pm 0.01}$	$56.26_{\pm 0.44}$	$41.64_{\pm 0.10}$
Peri-LN	3.288	42.62	50K	<b>31.63</b> $_{\pm 0.32}$	<b>63.07</b> $_{\pm 0.43}$	$32.05_{\pm 0.17}$	$32.40_{\pm 0.80}$	$49.41_{\pm 1.64}$	$24.91_{\pm 0.00}$	$58.05_{\pm 0.34}$	$41.65_{\pm 0.12}$
LNS	3.281	37.65	49K	$31.39_{\pm 0.24}$	$62.94_{\pm 0.64}$	<b>32.80</b> $_{\pm 0.16}$	$33.50_{\pm 0.58}$	$50.37_{\pm 0.91}$	$24.88_{\pm 0.01}$	$56.67_{\pm 0.37}$	$41.79_{\pm 0.26}$
BHyT	3.289	<b>33.22</b>	<b>46K</b>	$30.50_{\pm 0.16}$	$62.42_{\pm 0.41}$	$32.11_{\pm 0.10}$	<b>33.88</b> $_{\pm 0.73}$	$50.15_{\pm 0.34}$	$25.19_{\pm 0.02}$	<b>61.86</b> $_{\pm 0.17}$	<b>42.30</b> $_{\pm 0.13}$
Llama-3B											
Method	PT Train Loss	Wall time (hour)	Checkpoint Step	Arc-e	PIQA	Hellaswag	OpenBookQA	Winogrande	MMLU	BoolQ	Avg.
RMSNorm	3.203	76.55	60K	$31.01_{\pm 0.21}$	<b>66.57</b> $_{\pm 0.41}$	<b>41.52</b> $_{\pm 0.25}$	<b>33.92</b> $_{\pm 0.33}$	$50.50_{\pm 0.78}$	$25.67_{\pm 0.02}$	$37.94_{\pm 0.12}$	$40.89_{\pm 0.18}$
Peri-LN	3.165	88.72	60K	$31.82_{\pm 0.38}$	$64.52_{\pm 0.24}$	$36.05_{\pm 0.11}$	$32.28_{\pm 0.59}$	$49.30_{\pm 0.52}$	$25.99_{\pm 0.00}$	$57.46_{\pm 0.31}$	<b>42.49</b> $_{\pm 0.25}$
LNS	3.160	78.55	60K	<b>31.88</b> $_{\pm 0.42}$	$64.68_{\pm 0.46}$	$36.25_{\pm 0.10}$	$32.45_{\pm 0.53}$	$51.18_{\pm 0.75}$	<b>26.87</b> $_{\pm 0.01}$	$37.83_{\pm 0.08}$	$41.16_{\pm 0.11}$
BHyT	3.135	<b>64.30</b>	<b>56K</b>	$31.84_{\pm 0.15}$	$65.08_{\pm 0.39}$	$36.48_{\pm 0.04}$	$31.76_{\pm 0.33}$	<b>51.62</b> $_{\pm 0.66}$	$25.70_{\pm 0.01}$	<b>60.84</b> $_{\pm 0.29}$	<b>43.33</b> $_{\pm 0.16}$

To assess how efficiently each normalization method reduces loss during pretraining, we measure the time required to reach the loss achieved by BHyT approximately 5,000 steps before its training is completed. For both the Llama-1B and Llama-3B models, we track this target loss and evaluate competing methods at the point when (and if) they reach it. As shown in Table 6, most baselines reach this loss only much later in training or fail to reach it at all within the allotted training budget, indicating substantially slower effective convergence. Peri-LN, selected as the strongest stability-oriented baseline, eventually approaches the target loss but requires notably more wall-clock time due to the additional normalization applied before and after each sublayer. RMSNorm and LNS converge more slowly and often do not reach the target loss during pretraining. DyT is excluded from this comparison. Although DyT achieves higher throughput in training time, it remains highly sensitive to hyperparameter choices and does not consistently reduce pretraining loss, making it unsuitable for a meaningful time-to-loss comparison. Overall, BHyT reaches the target loss significantly earlier than all baselines while maintaining competitive downstream accuracy, demonstrating that BHyT provides both stable and efficient optimization at scale.



(a) Average per-layer variance in Llama-1B for DyT and BHyT under different learning rates.



(b) Pretraining loss curves of DyT and BHyT for different learning rates.

Figure 5: Learning-rate robustness of DyT and BHyT with tanh-based method in Llama-1B. (a) Average per-layer variance as a function of depth under different learning rates; DyT exhibits rapidly increasing variance at larger learning rates, while BHyT maintains a much smaller variance that grows roughly linearly with depth. (b) Pretraining loss versus training tokens for DyT (left) and BHyT (right) across learning rates, where BHyT converges stably over a wide range of learning rates.

D.2 TRAINING STABILITY UNDER VARYING LEARNING RATES: DYT VS. BHyT

We compare the training stability of DyT and BHyT, which replace the normalization layer with a tanh-based layer when the learning rate is varied. Figure 5 shows that, for DyT, increasing the learning rate leads to a sharp growth in variance amplification, making pretraining harder to converge. In contrast, BHyT exhibits a much smaller variance scale that grows roughly linearly with depth, and its pretraining converges stably across a wide range of learning rates. These results indicate that BHyT offers robust training stability for large-scale models such as LLMs, enabling more efficient and reliable hyperparameter sweeps.

D.3 VARIANCE APPROXIMATION

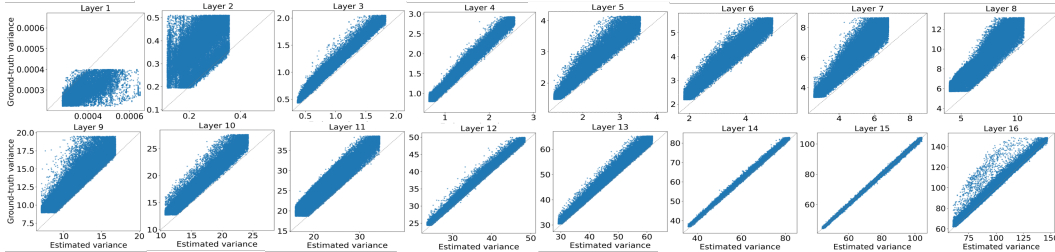


Figure 6: Full layer-wise comparison between the approximated and ground-truth activation variances for the second BHyT layer across all Transformer blocks in Llama-1B. Each subplot corresponds to one layer and shows the estimated variance against the empirical variance computed from randomly sampled C4 inputs.

Figure 6 presents a layer-wise comparison between the approximated and ground-truth activation variances for the second BHyT layer across all Transformer blocks in Llama-1B. Table 7 summarizes the quantitative evaluation, showing low RMSE and high  $R^2$ , Pearson correlation  $r$ , and Spearman

Table 7: Evaluation of the variance approximation. RMSE quantifies the discrepancy between the approximated and ground-truth variances, while the coefficient of determination  $R^2$  measures how well the approximation explains the variability of the ground-truth values. The Pearson correlation coefficient  $r$  and the Spearman rank correlation  $\rho$  assess linear and rank-based associations, respectively. Higher values of  $R^2$ ,  $r$ , and  $\rho$  indicate better approximation performance.

RMSE	$2.124_{\pm 5e-2}$
$R^2$	$0.99_{\pm 4e-5}$
$r$	$0.99_{\pm 1e-5}$
$\rho$	$0.99_{\pm 5e-5}$

rank correlation  $\rho$ , which together indicate that the approximation accurately captures both the scale and structure of the true variances.

#### D.4 TOKEN GENERATION SPEED

Table 8: Comparison of generation throughput (tokens/s). Values represent mean  $\pm$  standard deviation for five trials, and percentages in parentheses denote the relative speed difference compared to BHyT. The results demonstrate that BHyT achieves competitive inference speeds, consistently outperforming normalization-based baselines.

Throughput (tokens/s)	Max new token length		
	128	512	1024
RMSNorm	$50.5_{\pm 1.1}$ (-5.6%)	$38.0_{\pm 0.3}$ (-3.6%)	$30.1_{\pm 0.2}$ (-3.5%)
Peri-LN	$46.6_{\pm 0.7}$ (-12.9%)	$34.5_{\pm 0.0}$ (-12.4%)	$27.0_{\pm 0.1}$ (-13.5%)
LNS	$50.6_{\pm 0.5}$ (-5.4%)	$37.4_{\pm 0.2}$ (-5.1%)	$29.5_{\pm 0.1}$ (-5.4%)
DyT	$55.6_{\pm 0.2}$ (+3.9%)	$40.2_{\pm 1.3}$ (+2.0%)	$32.3_{\pm 0.2}$ (+3.5%)
BHyT	$53.5_{\pm 0.4}$	$39.4_{\pm 0.2}$	$31.2_{\pm 0.2}$

Table 8 shows the generation throughput (tokens/s) across different values of the maximum number of new tokens, showing mean  $\pm$  standard deviation over five trials and the relative speed difference with respect to BHyT. Across all generation lengths, BHyT consistently achieves higher throughput than normalization-based baselines, indicating that its inference-time advantage is maintained even as the maximum number of generated tokens increases.

## E PRETRAINING AND SFT RESULTS FOR LLAMA-1B

In the main text, we focused on the scalability of BHyT using the Llama-3B model. Here, we provide the detailed experimental results for the Llama-1B model under the same standard pretraining (Standard C4 budget) and SFT settings.

Table 9: Pretraining (PT)-only evaluation for Llama-1B. BHyT consistently achieves the lowest pretraining loss and superior average accuracy compared to baselines.

Llama-1B											
Method	PT Train Loss	PT Eval Loss	PT Eval PPL	Arc-e	PIQA	Hellaswag	OpenBookQA	Winogrande	MMLU	BoolQ	Avg.
RMSNorm	3.281	3.272	26.353	$30.97_{\pm 0.20}$	$62.89_{\pm 0.74}$	$32.77_{\pm 0.09}$	$32.32_{\pm 0.94}$	<b>50.54</b> $_{\pm 0.48}$	<b>25.70</b> $_{\pm 0.01}$	$56.26_{\pm 0.44}$	$41.64_{\pm 0.10}$
Peri-LN	3.288	3.279	26.545	<b>31.63</b> $_{\pm 0.32}$	<b>63.07</b> $_{\pm 0.43}$	$32.05_{\pm 0.17}$	$32.40_{\pm 0.80}$	$49.41_{\pm 1.64}$	$24.91_{\pm 0.00}$	$58.05_{\pm 0.34}$	$41.65_{\pm 0.12}$
LNS	<b>3.280</b>	<b>3.271</b>	<b>26.342</b>	$31.39_{\pm 0.24}$	$62.94_{\pm 0.64}$	<b>32.80</b> $_{\pm 0.16}$	$33.50_{\pm 0.58}$	<b>50.37</b> $_{\pm 0.91}$	$24.88_{\pm 0.01}$	$56.67_{\pm 0.37}$	<b>41.79</b> $_{\pm 0.26}$
DyT	3.709	3.696	40.294	$29.28_{\pm 0.48}$	$58.84_{\pm 0.58}$	$26.51_{\pm 0.20}$	$30.85_{\pm 0.87}$	$50.34_{\pm 0.68}$	$24.90_{\pm 0.00}$	$39.08_{\pm 0.31}$	$37.11_{\pm 0.11}$
BHyT	<b>3.268</b>	<b>3.254</b>	<b>25.908</b>	$30.50_{\pm 0.16}$	$62.42_{\pm 0.41}$	$32.11_{\pm 0.10}$	<b>33.88</b> $_{\pm 0.73}$	$50.15_{\pm 0.34}$	$25.19_{\pm 0.02}$	<b>61.86</b> $_{\pm 0.17}$	<b>42.30</b> $_{\pm 0.13}$

Regarding the inference speed, detailed comparisons for Llama-1B across different generation lengths are provided in Appendix D.4 and Table 8.

Table 10: Supervised fine-tuning (SFT) results for Llama-1B. BHyT maintains stable optimization and attains competitive accuracy on downstream benchmarks.

Llama-1B											
Method	PT Eval Loss	SFT Train Loss	SFT Eval Loss	Arc-e	PIQA	Hellaswag	OpenBookQA	Winogrande	MMLU	BoolQ	Avg.
RMSNorm	3.272	3.200 $\pm$ 0.011	3.664 $\pm$ 0.144	26.09 $\pm$ 0.13	50.58 $\pm$ 0.23	26.16 $\pm$ 0.07	30.56 $\pm$ 0.09	47.18 $\pm$ 0.51	26.66 $\pm$ 0.13	37.85 $\pm$ 0.03	35.01 $\pm$ 0.11
Peri-LN	3.279	3.113 $\pm$ 0.012	3.594 $\pm$ 0.147	26.68 $\pm$ 0.16	51.35 $\pm$ 0.10	25.76 $\pm$ 0.17	30.80 $\pm$ 0.24	48.79 $\pm$ 1.02	26.83 $\pm$ 0.10	57.16 $\pm$ 0.85	38.20 $\pm$ 0.25
LNS	3.271	3.118 $\pm$ 0.012	3.619 $\pm$ 0.145	27.26 $\pm$ 0.18	50.08 $\pm$ 0.22	24.80 $\pm$ 0.04	34.72 $\pm$ 0.18	50.94 $\pm$ 0.79	24.78 $\pm$ 0.01	37.83 $\pm$ 0.00	35.77 $\pm$ 0.12
DyT	3.696	3.226 $\pm$ 0.010	3.747 $\pm$ 0.135	30.98 $\pm$ 0.07	59.53 $\pm$ 0.15	27.08 $\pm$ 0.13	27.64 $\pm$ 0.26	50.56 $\pm$ 0.66	25.10 $\pm$ 0.08	60.68 $\pm$ 0.43	40.22 $\pm$ 0.21
BHyT	<b>3.254</b>	<b>2.841</b> $\pm$ 0.012	<b>3.288</b> $\pm$ 0.132	<b>32.49</b> $\pm$ 0.22	<b>64.04</b> $\pm$ 0.13	<b>32.53</b> $\pm$ 0.10	30.76 $\pm$ 0.54	50.92 $\pm$ 0.45	24.64 $\pm$ 0.04	<b>62.01</b> $\pm$ 0.05	<b>42.48</b> $\pm$ 0.07

## E.1 PRETRAINING RESULTS OF LLAMA-1B ON 20B TOKENS

Table 11: Performance of Llama-1B pretrained on 20B tokens, evaluated before and after supervised fine-tuning (SFT). BHyT consistently outperforms the stability-oriented baseline, Peri-LN, achieving lower losses and higher downstream accuracy.

Llama-1B (Pretrained on 20B tokens only)													
Method	PT Train Loss	PT Eval Loss	PT Wall time	SFT Tr Loss	SFT Eval Loss	Arc-e	PIQA	Hellaswag	OpenBookQA	Winogrande	MMLU	BoolQ	Avg.
Peri-LN	2.870	2.846	161.7h	-	-	37.91 $\pm$ 0.23	69.16 $\pm$ 0.33	46.77 $\pm$ 0.10	31.36 $\pm$ 0.82	50.89 $\pm$ 0.96	27.71 $\pm$ 0.00	51.74 $\pm$ 0.63	45.08 $\pm$ 0.09
BHyT	<b>2.828</b>	<b>2.802</b>	<b>135.0h</b>	-	-	<b>40.98</b> $\pm$ 0.43	69.13 $\pm$ 0.34	<b>49.00</b> $\pm$ 0.07	30.56 $\pm$ 0.73	50.67 $\pm$ 0.75	26.83 $\pm$ 0.00	<b>55.86</b> $\pm$ 0.38	<b>46.15</b> $\pm$ 0.23
Llama-1B (Pretrained on 20B tokens & SFT)													
Peri-LN	2.870	2.846	161.7h	2.522 $\pm$ 0.011	2.856 $\pm$ 0.107	47.90 $\pm$ 0.63	71.09 $\pm$ 0.35	47.79 $\pm$ 0.24	31.24 $\pm$ 0.52	51.98 $\pm$ 0.48	26.68 $\pm$ 0.01	48.74 $\pm$ 0.79	46.44 $\pm$ 0.27
BHyT	<b>2.828</b>	<b>2.802</b>	<b>135.0h</b>	2.550 $\pm$ 0.011	<b>2.825</b> $\pm$ 0.112	<b>49.23</b> $\pm$ 0.60	71.02 $\pm$ 0.28	<b>49.42</b> $\pm$ 0.15	30.72 $\pm$ 0.84	51.49 $\pm$ 0.80	<b>27.36</b> $\pm$ 0.01	<b>54.83</b> $\pm$ 0.94	<b>47.72</b> $\pm$ 0.31

Table 11 compares BHyT and Peri-LN on the Llama-1B architecture pretrained on 20B tokens. Consistent with results on larger models, BHyT shows superior training efficiency, reducing wall-clock time from 161.7 to 135.0 hours. Despite this speedup, BHyT achieves better convergence, with lower training and evaluation losses in both pretraining and SFT. Moreover, BHyT attains higher average downstream accuracy under both settings (Pretraining only and Pretraining & SFT), indicating that its stability and efficiency benefits scale well with increased training tokens.